AL-Bahir
Journal for Engineering and Pure Sciences
BJEPS

Volume 8 | Issue 2 Article 9

Plant-Mediated Green Synthesis of Zinc Ferrite Nanoparticles: Mechanisms, Properties, and Advanced Applications in Environmental and Biomedical Fields

Rihab Jabbar
Institute of Technology, Middle Technical University, Baghdad, Iraq.

REVIEW

Plant-Mediated Green Synthesis of Zinc Ferrite Nanoparticles: Mechanisms, Properties, and Advanced Applications in Environmental and Biomedical Fields

Rihab Jabbar

Institute of Technology, Middle Technical University, Baghdad, Iraq

Abstract

Recently, plant-mediated green synthesis has emerged as a sustainable, eco-friendly, and cost-effective strategy for synthesizing zinc ferrite ($ZnFe_2O_4$) nanoparticles (NPs). This review critically examines the advancements in bio-synthesizing $ZnFe_2O_4$ NPs using various plant extracts, including *Aloe vera, Hibiscus rosa-sinensis, Aegle marmelos, Eucalyptus leaves, Tragacanth gum, Piper nigrum, and Moringa oleifera*, among others. It emphasizes their dual role as reducing, capping, chelating, and stabilizing agents. The article extensively compares physicochemical properties of the green-synthesized NPs in terms of crystallite size, morphology, magnetic behavior, and band gap energy. Achieved through different synthesis routes such as sol-gel, hydrothermal, co-precipitation, and microwave-assisted methods. Special attention is given to the roles of phytochemicals, reaction conditions (pH and temperature, etc.), and post-treatment parameters in tuning the properties of NPs. Moreover, the review highlights the multifunctional applications of bio-synthesized $ZnFe_2O_4$ NPs in photocatalytic degradation of organic dyes, antimicrobial activity against pathogenic strains, anticancer uses, and their integration as anode materials in lithium-ion batteries. Through a structure-function correlation analysis, this study establishes $ZnFe_2O_4$ NPs as a promising platform for green nanotechnology, with significant implications for environmental remediation and biomedical innovation.

Keywords: Green synthesis, Zinc ferrite, Plant extract, Biomedical application, Antibacterial activity, Anticancer activity, Water treatment

1. Introduction

Nanotechnology is the study of working with materials at the atomic and/or molecular level, as well as creating and using materials that are 0.000000001 m in size. Unlike their bulk matter, nanoparticles (NPs) are microscopic particles with a typical 1−100 nm dimension span [1]. They exhibit unique chemical, physical, mechanical, magnetic, and electrical characteristics, making them appropriate for various applications. The high surface-to-volume area of NPs can be used extensively in various disciplines, such as biomedical, industrial, wastewater treatment, bio-diesel, and lithium batteries. Agglomeration presents one of the main challenges in the synthesis of NPs. It could be decreased by encasing the NPs in a polymeric matrix or by coating their surfaces with a surfactant to prevent agglomeration [2,3].

Numerous methods have been developed to prepare NPs. Briefly, the “top-down” process, such as ball milling and laser ablation, uses lithographic techniques and mechanical methods like grinding to reduce the size of bulk material to produce NPs. In contrast, the “bottom-up” process, such as co-precipitation, sol-gel, and microemulsion, uses smaller building NPs from atomic/molecular levels to create a larger structure with greater control over size and shape [4]. Both conventional chemical and physical routes for preparing NPs have drawbacks

Received 2 November 2025; revised 1 January 2026; accepted 10 January 2026.
Available online 3 April 2026

E-mail address: rihab_jabbar@mtu.edu.iq.

https://doi.org/10.55810/2313-0083.1126

such as high manufacturing costs, used toxic chemicals, high energy requirements, Insafe for the environment. Some chemicals are utilized in chemical synthesis techniques (such as sol-gel and hydrothermal), which can create dangerous by-products and impurities from the starting compounds. As a result, the need for safe, non-toxic, and environmentally friendly NPs synthesis techniques is growing. Presently, a new integrated scientific direction, known as "green synthesis," marks the beginning of a new era in the history of NPs synthesis techniques. To reduce environmental hazards and try to prevent pollution as early as possible in the planning and execution stages, green synthesis encompasses all types and aspects of chemical processes. It aims to create technologies for processing chemical reactions more effectively and utilizing waste from the environmentally hazardous chemical industry outputs [5–7]. In their 1998 book "Green Chemistry: Theory and Practice," John W. and Paul A. coined the term "Green Chemistry." see Fig. 1, green chemistry encompasses the following 12 principles: preventing waste, minimizing the number of components (the "atom economy"), developing less hazardous chemical syntheses, designing safe chemicals and products, using safe solvents and reaction conditions, using renewable raw materials, avoiding chemical derivatives, using non-stoichiometric catalysts, designing degradable chemicals and products, reducing the likelihood of accidents, reducing the likelihood of accidents, and designing safer chemicals and their physical forms (solid, liquid, or gaseous).

This review stands out for its comprehensive analysis of green synthesis methods that utilize plants extract to produce zinc ferrite NPs. Its primary emphasis is on highlighting the significance of green chemistry in advancing sustainability. Additionally, it draws attention to the advantages of $ZnFe_2O_4$ NPs, which are generated through straightforward, cost-effective, and non-hazardous processes for various advanced applications such as environmental remediation and biomedical uses.

2. The review novelty

We explore the trend of synthesizing $ZnFe_2O_4$ NPs over time, starting from the first published

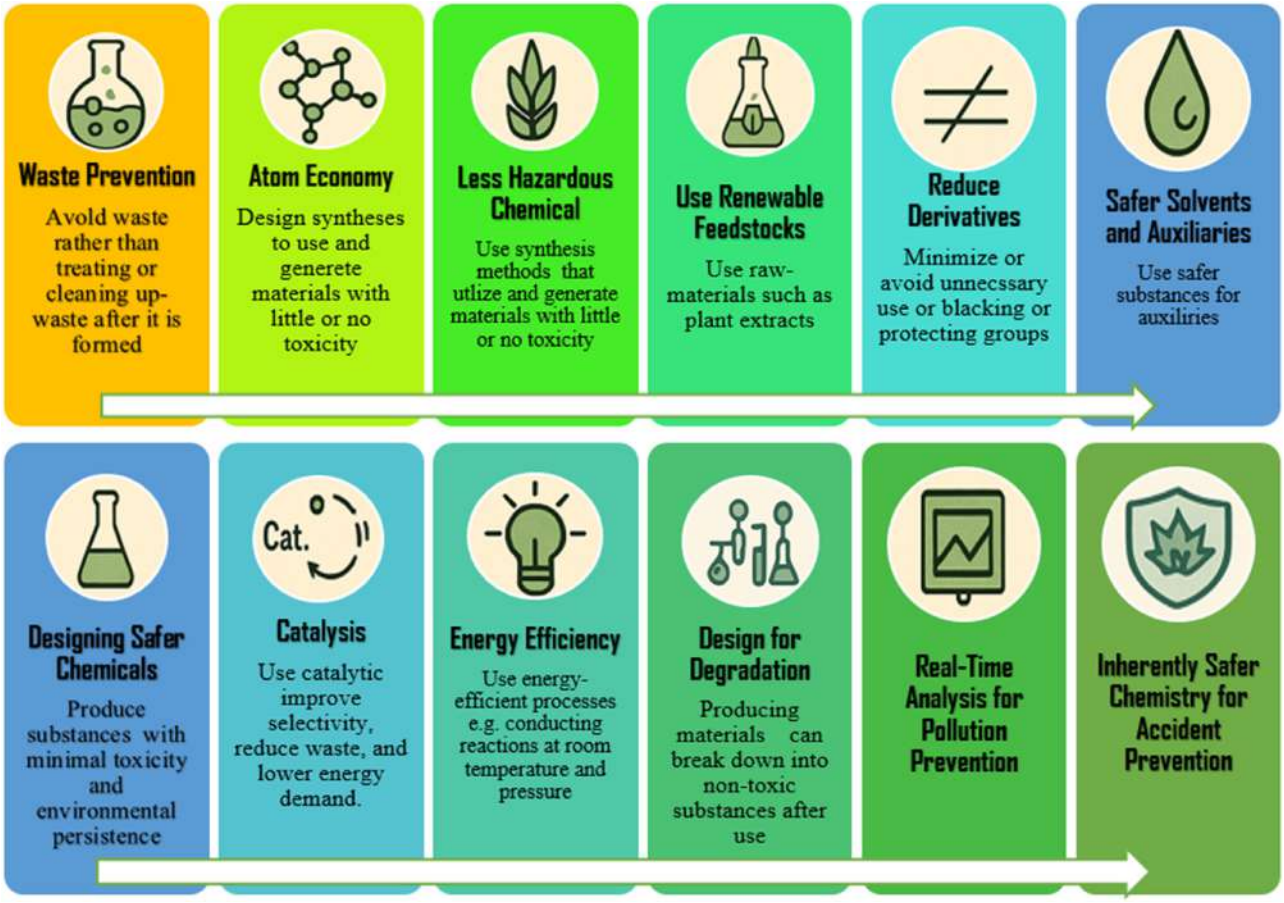

Fig. 1. Principles of green chemistry.

article in 1993 by Blums et al. [8], according to the Scopus database. Since then, research has focused on synthesizing $ZnFe_2O_4$ NPs, with increasing interest in the last ten years due to their unique properties and wide applications in fields such as industry and biomedicine. Additionally, biosynthesis has become an innovative method for producing $ZnFe_2O_4$ NPs, gaining significant attention over the past 20 years. This approach aligns with the 12 principles of green chemistry mentioned above. Recently, there has been growing interest in synthesizing $ZnFe_2O_4$ NPs using green sources such as plant extracts, bacteria, and fungi (see Fig. 2). Therefore, the novelty of this work can be summarized as follows:

I. Unlike published review papers, this review offers a detailed comparison of the green synthesis of $ZnFe_2O_4$ NPs using plant extracts. It also focuses on the impact of phytochemical biogenic components on the structural, morphological, optical, magnetic, and other properties of $ZnFe_2O_4$ NPs.
II. In contrast to conventional techniques such as the sol-gel route, co-precipitation, ball milling, hydrothermal, etc., this evaluation specifically assesses these methods in terms of cost-effectiveness, safety, and environmental sustainability.
III. Explore the performance of these NPs in various applications. Prioritize environmental applications, such as photo-catalysis, water treatment, and Ion-lithium batteries, which have been underrepresented in previous assessments, in addition to biomedical applications, such as anticancer agents and antimicrobial activity.
IV. Also, this review presents the current challenges and limitations and the future directions of this green technology in synthesizing $ZnFe_2O_4$ NPs and their performance in the mentioned fields.pt

3. Spinel ferrite

Spinel ferrite is also called cubic ferrite, as shown in Fig. 3. Are the most commonly utilized family of ferrites. Their low eddy current losses and high electrical resistance make them perfect for use in microwave frequencies. In 1915, Bragg and Nishikawa determined the ferrite spinel structure for the first time. It is a structure similar to the mineral spinel $MgAl_2O_4$. A spinel ferrite's general chemical composition can be expressed as MFe_2O_4, where "M" is any divalent metal ion, like Fe^{+2}, Co^{+2}, Ni^{+2}, Cu^{+2}, Mg^{+2}, Cd^{+2}, Zn^{+2}, or a mixture of these ions. Spinel ferrite has an FCC unit cell, which has eight formula units. $M_8Fe_{16}O_{32}$ is one way to write the formula. With the largest anions, an FCC lattice is formed. The metallic cations occupy two sorts of interstitial locations found inside these lattices. The unit cell has (96) interstitial sites, (64) of which are tetrahedral (A) sites, and the rest (32) are octahedral (B) sites. The cation distribution on the tetrahedral (A) and octahedral (B) sites of spinel ferrite has led to its classification into three groups: mixed, inverse, and normal [9–11].

3.1. Normal spinel

The spinel is normal if only one kind of cation is on the octahedral (B-sites). The trivalent cations in these ferrites are on the octahedral (B-sites), whereas the divalent cations are on the tetrahedral

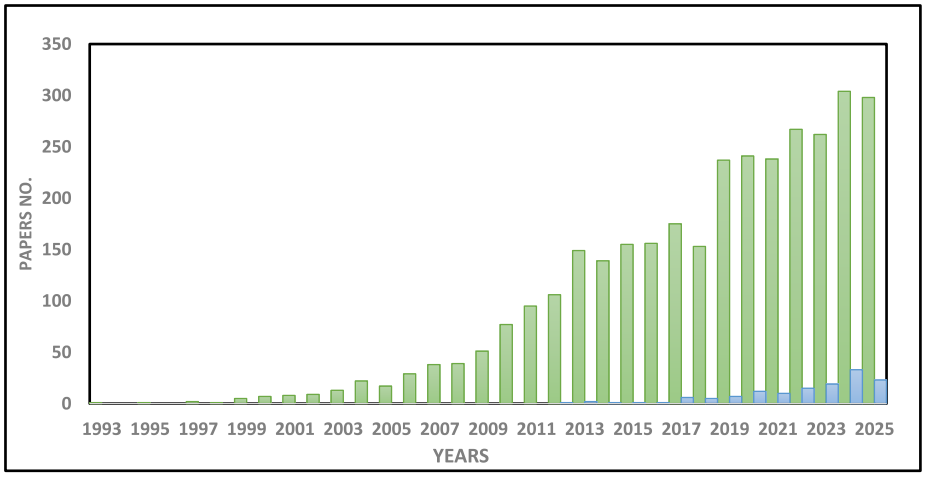

Fig. 2. The number of published articles of $ZnFe_2O_4$ NPs synthesized via a conventional method or green routes in the Scopus database from 1993 until 2025. Using these keywords "zinc ferrite nanoparticles" and "green synthesis of zinc ferrite nanoparticles".

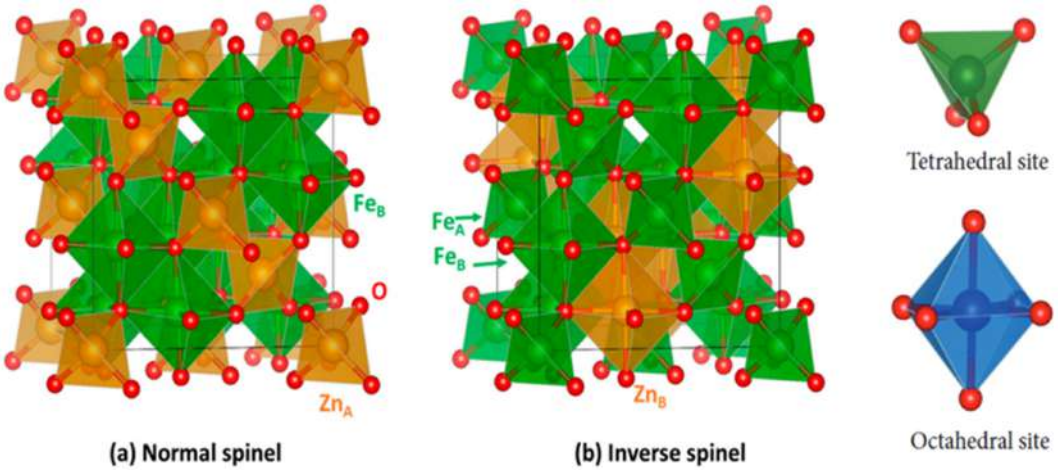

Fig. 3. Shows the crystal structure of spinel ferrite NPs and the tetrahedral (A-site) and octahedral (B-site).

(A-sites). $(M^{+2})_A[M_e^{+3}]_BO_4$ is the general formula represent normal spinel. Where M_e denotes trivalent ions, and M denotes divalent ions. Bulk $ZnFe_2O_4$ is an example of a standard spinel ferrite (see Fig. 3) [9,10].

3.2. Inverse spinel

In this configuration, half of the trivalent ions are located in octahedral (B-sites), and the other half in tetrahedral (A-sites). Remaining cations are dispersed in the octahedral (B-sites). These ferrites are expressed using the formula $(Fe^{+3})_A[M^{+2}Fe^{+3}]_BO_4$. Fe_3O_4 is a common instance of inverse spinel ferrite (see Fig. 3) [9,10,12].

3.3. Mixed spinel

Mixed spinel is defined as spinel with an ionic distribution that is halfway between normal and inverse, for example, $(M_{—}^{+2}\ Me^{+2}{}_{1-—})_A\ [M_{1-—}^{+2}\ Me_{1+—}^{+3}]_BO_4$, where —is the inversion parameter. The amount —depends on the ferrites' constituents' type and preparation technique. For mixed spinel ferrite, —varies between ($0 < — < 1$). Where ($— = 1$) for the entire inverse spinel ferrite, oppositely, ($— = 0$) for the complete normal spinel ferrite. If the spinel has an uneven distribution of cations on its octahedral sites, it is considered mixed ferrite. The minerals $MgFe_2O_4$ and $MnFe_2O_4$ are common examples of mixed spinel ferrites [9,10,13].

4. Hexagonal ferrites

Because of their strong coercivity (Hc), hexagonal ferrites are frequently utilized as permanent magnets. The general formula is $MO•6Fe_2O_3$, in which M may be Ba, Sr, or Pb. With oxygen ions closely packed, the hexagonal ferrite lattice resembles the spinel structure. However, metal ions are present in some layers, with ionic radii almost identical to oxygen ions. Three distinct metal sites, tetrahedral, octahedral, and trigonal bipyramid (encircled by five oxygen ions), are present in this lattice [14].

5. Garnets

Garnet ferrites (GF) exhibit a crystal structure identical to the silicate mineral garnet. GF has a dodecahedral or twelve-sided structure related to mineral garnet with general formula $Me_3Fe_5O_{12}$. Notably, all the metal ions in this class of ferrites are trivalent, distinguishing them from other ferrite categories. In most GF, the main constituents are one of the rare earth ions or yttrium ions. Bertaut and Forrat first reported the crystal structure and unit cell dimensions for rare-earth iron garnets, later confirmed by Geller and Gileo [15]. The substitution of Y^{+3}, Al^{+3}, and Si^{+4} in the hexagonal ferrite structure produced the first silicon-free garnet ferrite ($Y_3Al_5O_{12}$). The structure of GF is exceptionally stable since all the cation-occupied sites contribute to the compound's high stability [15,16].

6. Zinc ferrite

Magnetic ferrites have received phenomenal attention due to their compatibility with modern technologies. Among magnetic ferrites, zinc ferrites ($ZnFe_2O_4$) have been widely used on an industrial level in various applications like supercapacitors, magneto-sensors, batteries, hydrogen sensors, gas sensors, photocatalysis, and drug delivery, sensing applications, magnetic resonance imaging and

antibacterial applications, etc. due to their unique properties including extremely high chemical stability, superior magnetic properties, resistivity, non-toxicity for living organisms, a narrow bandgap of about 1.67–2 eV and is capable of absorbing visible light and environmental safety [17–19]. While nanocrystalline $ZnFe_2O_4$ has a mixed spinel structure with metal ions over both of the A- and B-sites, displays exceptional magnetic characteristics compared to bulk $ZnFe_2O_4$, which has a spinel structure with tetrahedral (A-sites) occupied by Zn^{2+} and octahedral (B-sites) occupied by Fe^{3+} in the oxygen lattice (see Fig. 3) [20–22].

Because of its unique features, $ZnFe_2O_4$ NPs find application in numerous fields such as photo-catalyst, and gas sensor (for some gases such as acetone, ethanol vapor, etc.) [23,24]. Excellent electrochemical qualities like good cycling performance, high reversible specific capacity, high specific capacity, and good rate capability make $ZnFe_2O_4$ NPs a good candidate for a lithium-ion battery as an anode electrode [25,26]. Fig. 4 shows properties, synthesis methods, and applications of $ZnFe_2O_4$ NPs.

7. Preparation methods for zinc ferrite

It is possible to prepare $ZnFe_2O_4$ NPs through chemical or physical synthesis methods. A wide variety of magnetic NPs have been produced using several different methods. This section introduces and reviews traditional methods for manufacturing spinel ferrite $ZnFe_2O_4$ NPs.

7.1. Sol-gel method

The sol-gel approach is a novel technique for synthesizing nanostructured ferrite materials, such as $ZnFe_2O_4$ NPs, through a chemical solution process. A sol is a suspension of solid particles in a solvent, while a gel forms when the solvent evaporates, creating a semi-rigid network of particles. This method produces homogeneous NPs in colloidal powder, making it cost-effective and efficient at moderate temperatures. However, it requires thermal treatment to achieve high-purity and crystalline NPs, as the quality of the final product depends on the precursors used in the initial colloidal solution [27–29]. The sol-gel method synthesizes solid inorganic materials from a solution, typically using metal-organic compounds like metal alkoxides or inorganic metal salts. Alkoxides are advantageous due to their availability and ease of purification. They react with water to produce hydroxide and oxide precipitates, with particle sizes ranging from 0.01 to 1 m. The process involves hydrolysis and polymerization to create a sol, forming a gel. This gel can be processed into various forms, including powders and thin or thick films, using dip or spin coating. Fig. 5

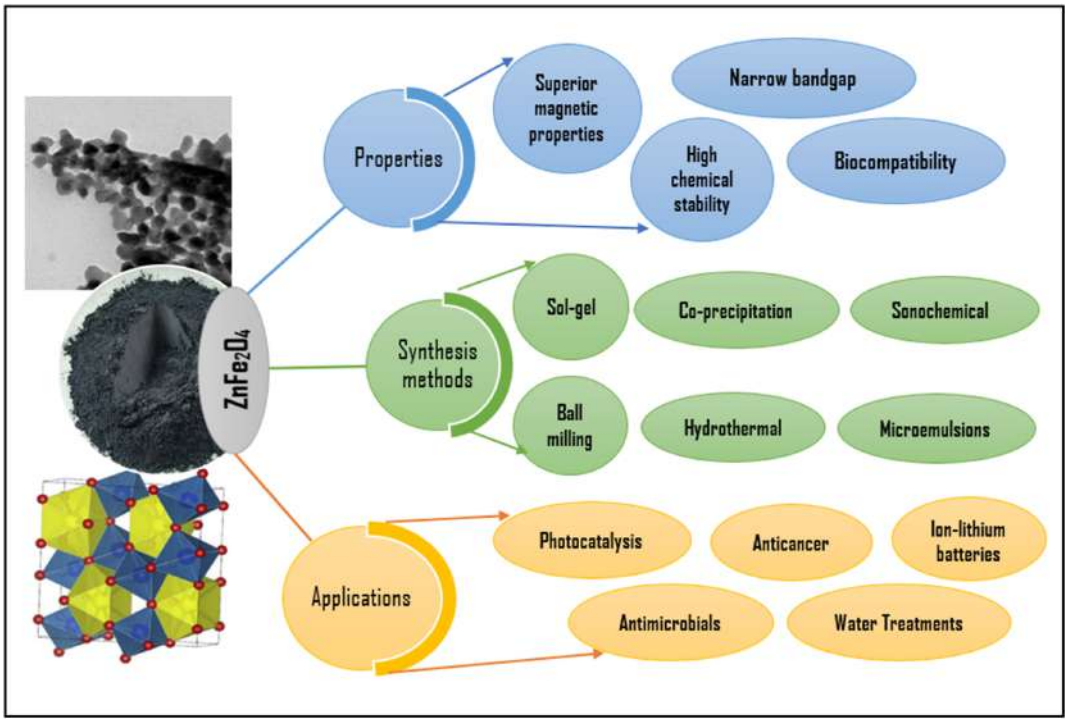

Fig. 4. Shows properties, synthesis methods, and applications of $ZnFe_2O_4$ NPs.

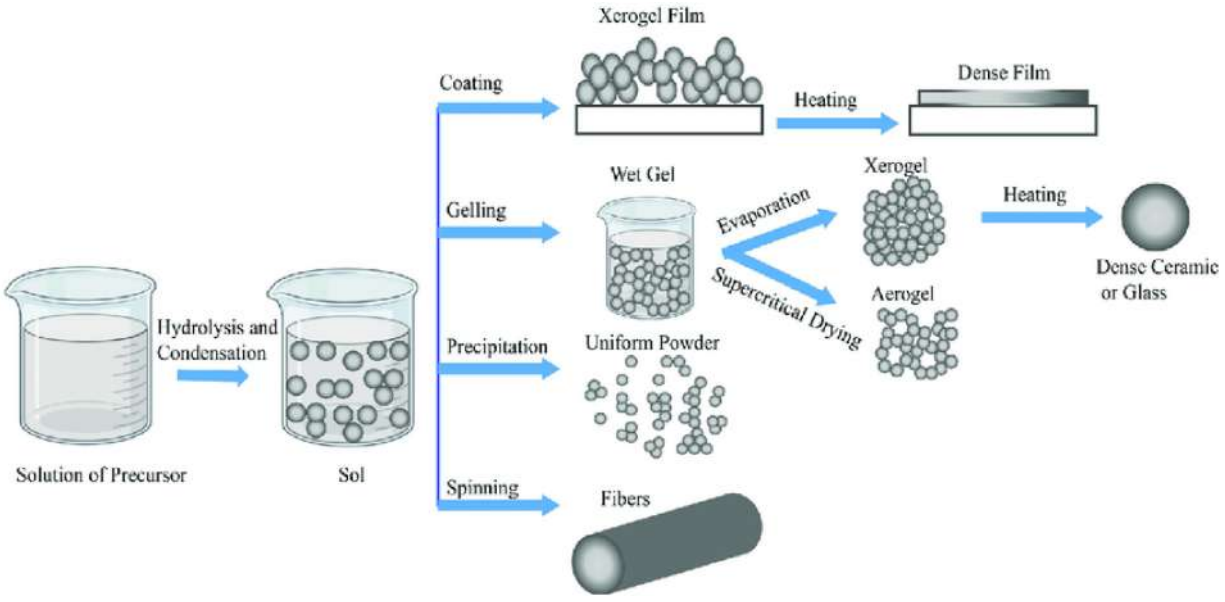

Fig. 5. The overall sol-gel process.

illustrates the comprehensive procedures involved in the sol-gel approach.

7.2. Co-precipitation method

The co-precipitation approach is often used for synthesizing NPs. Typically, this approach utilizes inorganic salts (such as nitrate, chloride, sulphate, etc.) as a starting material. These salts are dissolved in water and/or alcohol to create a uniform solution in an acidic or alkaline environment. Then the solvent is evaporated to obtain the NPs precipitates. Salt concentration, temperature, and pH level directly affected the formation of crystals and the aggregation of particles. Next, precipitation is heated to the temperature at which the medium boils to remove any remaining moisture and create hydroxides. Subsequently, the hydroxides undergo calcination to convert into crystalline oxides [30,31] The main challenge associated with the co-precipitation approach is the NPs' low crystallinity. However, this issue can be addressed by subjecting the NPs to additional heat treatment [32].

7.3. Hydrothermal method

The hydrothermal method utilizes high-pressure reactors or autoclaves to create elevated pressures/temperatures. This method allows for precise control over the size and shape of the NPs, eliminating the need for post-annealing treatment. This method involves the utilization of either aqueous or non-aqueous solutions under conditions of elevated temperatures and pressures to inhibit the occurrence of dislocation formation. Furthermore, this procedure enables the production of magnetic NPs possessing elevated vapor pressure at their respective melting temperatures while maintaining precise control over the compositions. This method is advantageous for producing spinel ferrite with empty interiors and precisely regulated shapes [33,34]. A benefit of this method is that it allows for manipulating and controlling particle size, morphology, and other physical characteristics. The reaction temperature, time, dopants, and other variables can influence the NPs' properties [35,36].

7.4. Microemulsions

Microemulsions are transparent, homogeneous blends of water, oil, and a surfactant that exhibit stability and clarity. This technique employs surfactants to facilitate the simultaneous presence of two liquids that cannot mix in a single homogeneous phase. Water/oil is one of the solvents utilized in microemulsion, where it is employed to create the solution by dispersing immiscible solvents. The manufacture of magnetic NPs commonly involves two widely used microemulsion methods: reverse, where water is dispersed in oil (w/o), and direct, where oil is dispersed in water (o/w) [32,37]. The benefit of this approach lies in its simplicity in resizing MFe_2O_4 NPs by modifying the particles to sizes smaller than a nanometer. Further, the microemulsion process yields diverse forms and a wide variety of sizes. The synthesis process for

spinel ferrite NPs has a low yield and a limited operating range compared to alternative approaches. Conversely, multiple studies have produced positive results when expanding the process for an economic or environmental facility [38,39].

7.5. Sonochemical methods

Sonochemical approaches utilize high-intensity ultrasound irradiation to exploit the chemical processes induced by sonic cavitation, producing distinct magnetic ferrite NPs morphologies. Ultrasonic irradiation induces the formation of bubbles that undergo continuous compression and expansion, resulting in the oscillation of the bubbles. Ultrasonic energy builds up within the pulsating bubbles, which gradually expand until they collapse, releasing the stored energy. When the bubbles break, there is a sudden and intense release of energy in a small area, causing a rapid and large increase in temperature and pressure [40,41]. The sonochemical approach showing promise in producing magnetic NPs with exceptional magnetic saturation capabilities. Also, faces challenges in achieving a restricted size distribution during synthesis. The magnetic NPs produced using this method are frequently amorphous, porous, and clustered [42].

7.6. Physical synthesis methods

Most physical mechanisms in breaking down a bulk spinel ferrite material into NPs are top−down processes. Explosions of electrical wires, Laser target evaporation, and mechanical milling are well-known examples of physical procedures.

Friedrich Fischer pioneered ball milling in the late 19th century. Subsequently, the simplicity, versatility, and capacity for expansion of ball milling have established it as a fundamental technique in materials science and engineering domains [43]. Ball milling is a widely used technique for reducing particle size and enhancing material reactivity. The procedure employs a ball mill, a cylindrical chamber containing a grinding medium, such as balls, that rotates on its axis to get the appropriate level of fineness for the end product. The grinding media collide with the particles, resulting in a reduction in their size and the formation of a more uniform mixture [44,45]. It can produce superior powders, disperse NPs, and even synthesize intricate materials. Ball milling has various possible drawbacks, including the potential for pollution, creation of NPs with non-uniform morphologies, generation of noise, and extended durations for milling and cleaning processes [43,46,47]. Table 1 shows a comparison between the plant-mediated synthesis of NPs with conventional methods such as sol-gel, co-precipitation, etc., in terms of environmental impact, reaction conditions, and product quality, in addition to their disadvantages.

8. Mechanism of plant-mediated synthesis

The biosynthesis of NPs is defined as the utilization of natural and/or biological resources, including biomolecules derived from plants, bacteria, or fungi, as well as whole cells or cellular components, to facilitate the production of NPs from aqueous solutions of corresponding salts. This area of research has witnessed significant advancements over the past two decades. The field rapidly expands and diversifies, giving rise to numerous intriguing sub-disciplines. These processes are typically conducted in aqueous environments at atmospheric pressure and under ambient or slightly elevated temperatures. Moreover, no additional synthesis steps are necessary, as the metallic salts are utilized in their received form. These environmentally benign experimental approaches, which rely on natural resources, align with the 12 principles of Green Chemistry [52].

The plant-mediated synthesis of NPs has emerged as a promising, environmentally friendly alternative to traditional physical/chemical synthesis methods, owing to its ecological benefits, cost-effectiveness, and simplicity. This technique capitalizes on the abundant phytochemical constituents found in various parts of plants, including leaves, stems, fruits, flowers, and roots, serving dual roles as reducing and stabilizing agents for metal ions [49].

The synthesis process typically commences with the preparation of an aqueous extract of the selected plant material, wherein bioactive compounds such as flavonoids, terpenoids, phenolic acids, alkaloids, and proteins play a crucial role in the reduction of metal salts to zero-valent NPs. These bioactive compounds containing active functional groups include hydroxyl (OH^-), Carbonyl (C═O), and Carboxyl (−COOH), Amino/amide groups (NH_2^-, amide-O), and Aldehydes and reducing sugars (—CHO) in monosaccharides/polysaccharides. For instance, hydroxyl (OH^-) acts as a primary reducing agent of metal ions by donating their electrons and reducing the metal ions into their metal-zerovalent or lower valence state (Zn^{+2} — Zn^0), (Fe^{+2}/Fe^{+3} Fe^0/Fe^{+2}). Moreover, the hydroxyl group can act as a stabilizing species by adsorbing on NPs surfaces, and

Table 1. Represents a comparison between the green synthesis route (plant-mediated) and conventional methods such as sol-gel, co-precipitation, etc., in terms of environmental impact, reaction conditions, and product quality.

Method	Environmental Impact	Reaction Conditions	Product Quality	Disadvantages	Refs
Green synthesis (biological/ plant-mediated)	**Low:** Utilize water, Natural reducing and capping agents improved sustainability and minimized toxic reagents.	**Mild conditions**: Usually room−moderate temperature, aqueous media, No strong bases/acids, sometimes requires mild drying/calcination to improve crystallinity.	**Moderate−good**: Generally small size & stabilized by bio-capping, Surface functionalization enhances dispersion, Crystallinity and magnetic performance are typically lower than those of high-temperature methods unless post-sintering.	Phase purity, Extracts standardization, Scaling production up	[48−50]
Sol−gel	**Moderate:** Often uses organic solvents/ chelating agents, Requires energy for drying/ calcination.	Low to moderate synthesis temperatures, Gelation, then high-T calcination (typically 300 −1000 °C) to achieve crystalline spinel.	**Good**: high homogeneity, controlled stoichiometry, crystallinity and purity improve with calcination, particle sizes usually ~10 −50 nm	Time-consuming, weak bond formation, poor wear resistance	[32,51]
Co-precipitation	Lower than sol−gel, aqueous processing common, No organic solvents but requires careful pH neutralization/waste handling.	Room to moderate temperatures, Precipitation by base (pH control critical), Often short synthesis time, require post-annealing to enhance crystallinity.	**Moderate**: simple and inexpensive, Tends to yield particles ~20 −30 nm, size distribution can be broad without surfactants, Magnetic properties good after thermal treatment.	low crystallinity, Impurities, and longer time	[32,51]
Hydrothermal	**Moderate:** Aqueous solvent under pressure, No organic solvents required, Avoids high-T calcination in some protocols.	Elevated T (commonly 120 −250 °C) and autogenous pressure, Long reaction times (several hours).	**High**: Very uniform particle size (<20 nm often), high crystallinity, narrow distribution size, Enhanced phase purity, Good magnetic/functional performance.	High temperature and pressure	[32,51]
Microemulsion	Lower than many chemical routes: operates at mild T, Uses surfactants/organics with environmental disposal concerns, Careful surfactant management needed.	Mild T in controlled nanoscale droplets, surfactant systems stabilize nano-reactors, Reaction times can be several minutes to hours.	**High**: excellent control of size (~5−20 nm) with narrow size distribution, Well-defined morphology, Surfactant residues must be removed for optimal performance.	Low yield of product, difficult to obtain a uniform and stable emulsion system	[32,37]

providing steric and electrostatic stabilization [53]. Further, Aldehydes and reducing sugars (—CHO in monosaccharides/polysaccharides can also act as reducing/capping agents. Where the aldehydic groups reduce metal ions through the oxidation to carboxyls [54,55], Carbonyl (C═O) and Carboxyl (−COOH) groups act as capping and chelating agents through carboxylate coordinates, which bind the metal ions and control the nucleation and growth process and prevent the agglomeration [56]. Amino/amide groups (NH_2^-, amide-O) are excellent capping/stabilizing agents. It shares this ability through coordination, which forms a protein corona surrounding the NPs. In addition to their ability of certain side chains to contribute electrons (a possible reducing agent) [50,53]. Fig. 7 shows the chemical structure of plant phytochemicals and functional groups used in the green synthesis of NPs.

The bio-reduction process is initiated under ambient or moderately elevated temperatures when the plant extract is combined with a solution of metal precursors (such as metal nitrides or chlorides). The formation of NPs is often indicated by a discernible color change attributable to surface plasmon resonance (see Fig. 6-a). The reaction conditions, including pH, temperature, extract concentration and amount, and metal ion concentration, significantly affect the NPs' size, morphology, and physiochemical properties. The formed NPs are subsequently isolated through centrifugation and thoroughly washed to eliminate unbound phytochemicals, followed by drying or calcination, depending on the specific application intended [49,57,58].

The plant-mediated synthesis of metal oxide and ferrite NPs, such as $ZnFe_2O_4$ NPs, can be summarized using chemical equations 1–10. Herein, we suppose that the starting materials are metal nitrides such as ferric ($Fe(NO_3)_3 \bullet 9H_2O$) and zinc nitride ($Zn(NO_3)_2 \bullet 6H_2O$).

Dissolving the starting materials:

$$Fe(NO_3)_3 \cdot 9H_2O \quad Fe^{3+} + 3NO_3^- + 9H_2O \tag{1}$$

$$Zn(NO_3)_2 \cdot 6H_2O \quad Zn^{2+}\_aq + 2NO_3^-\_aq + 6H_2O \tag{2}$$

Complexation with phytochemicals

$$Zn^{2+} + x\,Phyt - L \quad [Zn(L)x]^{2+} \tag{3}$$

$$Fe^{3+} + y\,Phyt - L \quad {}^{\times}Fe(L)y^{3+} \tag{4}$$

Hydrolysis step

$${}^{\times}Zn\_Phyt - L\ x^{2+} + 2H_2O \quad M(OH)_2 + xPhyt - L + 2H^+ \tag{5}$$

$${}^{\times}Fe\_Phyt - L\ y^{3+} + 3H_2O \quad Fe(OH)_3 + yPhyt - L + 3H^+ \tag{6}$$

Thermal decomposition at relative low temperature (typically 60 °C–150 °C)

$$Zn(OH)_2 \quad ZnO + H_2O \tag{7}$$

$$Fe(OH)_3 \quad Fe_2O_3 + 1\,5H_2O \tag{8}$$

Solid-state formation at elevated temperature (typically 200 °C–1200 °C)

$$ZnO + Fe_2O_3 \quad ZnFe_2O_4 \tag{9}$$

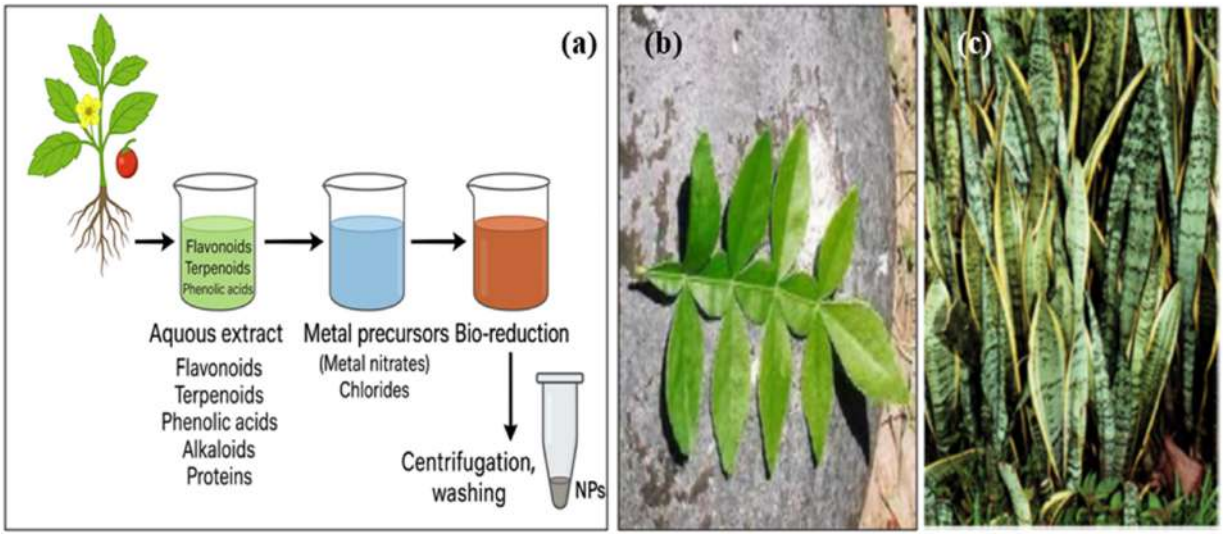

Fig. 6. (a) Typical Plant-mediated synthesis of NPs, (b) Aegle marmelos *leaves, and (c) Lidah mertua plant.*

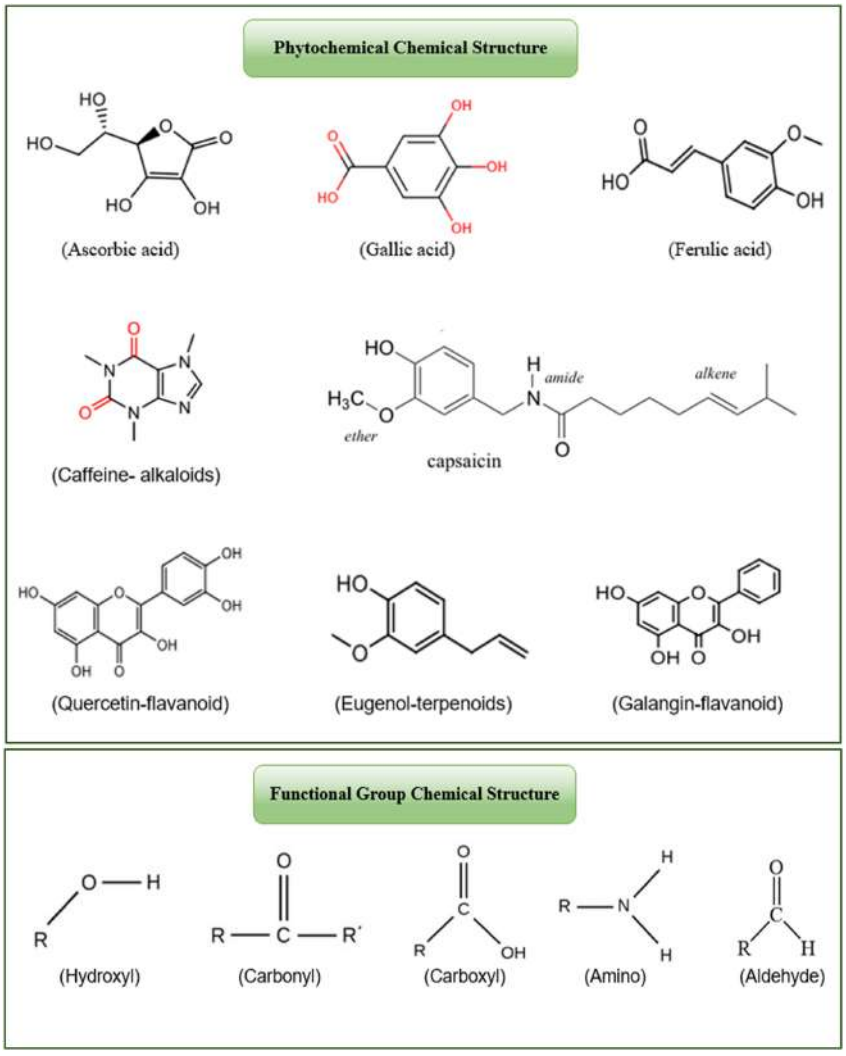

Fig. 7. The phytochemical and functional group chemical structure [59–62,69].

Overall reactions

$$Zn(NO_3)_2 \cdot 6H_2O + 2Fe(NO_3)_3 \cdot 9H_2O + \text{plant extract} \quad ZnFe_2O_4 \quad + 6HNO_3 + CO_2\&H_2O \qquad (10)$$

9. $ZnFe_2O_4$ NPs plant-mediated synthesis

For hundreds of years, people have been using plants as medicine. Numerous biological substances with anticancer properties can be found in medicinal plants. Antifungal, antibacterial, and other properties make them suitable for use as medications. Approximately 50,000 plant species are thought to have been researched and utilized for their therapeutic qualities [59,60]. Besides that, plants are diverse, affordable, scalable, and widely available. Therefore, bioreduction is highly encouraging [61]. Furthermore, every plant part can be used in the production of NPs. As a result, plant extracts attracted much attention as simple, useful, economical, and effective methods of producing NPs [62,63]. Flowers, leaves, and even seeds can all be used to make plant extracts. Additionally, it contains terpenoids, polyphenols, phenolic acids, proteins, carbs, and bioactive alkaloids. Each element serves various purposes, such as reducing, stabilizing, chelating, and capping agents [64,65]. Plants include all the physiologically active substances listed above, which can reduce metal ions far more quickly than bacteria or fungi [66,67]. P. Laokul et al. [68] used Aloe vera extract to synthesize $ZnFe_2O_4$ NPs via a sol-gel route. All samples have a polycrystalline nature with spinel structure, and the crystallite sizes increased from 15 nm to 70 nm with the raised calcination temperature (Tc). The morphological studies reveal that the $ZnFe_2O_4$ NPs have a uniform grain (100–130 nm), increasing

with increasing Tc, with a high tendency to agglomeration. Sarala et al. [69] utilized the sol-gel route to synthesize $ZnFe_2O_4$ NPs. *Lawsonia inermis* extract was used as a reducing agent. The results confirmed the formation of a spinel structure with a 17.12 nm crystal size. Moreover, homogeneous and agglomerated $ZnFe_2O_4$ NPs were observed by FESEM. The M–H loop explained that the samples have a superparamagnetic nature with magnetization (Ms) and coercivity field (Hc) of 42.9 emu/g and 11.9 Oe, respectively. *Hibiscus rosa-sinensis* plant extract modified conventional combustion (CCM) and microwave-assisted combustion (MCM) to prepare $ZnFe_2O_4$ NPs. The XRD results showed that the average crystallite size was 81 nm for CCM and 39 nm for MCM. The HRSEM micrograph showed that microwave-assisted processing positively affects the particles' homogeneity and uniformity. The particle size changed from 23.4 to 541.7 nm. The magnetic properties showed that both samples are superparamagnetic with a minimal Ms value of about 63.61–255.7 memu/g [21]. Kombaiah et al. [70] utilized the same two methods to synthesize $ZnFe_2O_4$ NPs. But at this time, the *Opuntia dilenii haw* extract was used as a reducing agent. The findings demonstrated no significant change in morphological and structural properties. The average crystallite size is 32–73 nm, with agglomerated grains and the Ms between 47.13 and 1024 memu/g. In actuality, these Ms values are extremely low when compared to other previous and recent studies [71–73] On the other hand, the green strategies used in these studies by Laokul, Sarala, and Kombaiah yielded valuable findings, indicating that using *Aloe vera*, *Lawsonia inermis, and Hibiscus rosa-sinensis* extracts as a reducing agent correlated with reducing hazardous chemicals, preventing waste material generation, and enhancing energy efficiency compared to conventional methods.

Korotkova et al. [74] utilized the *Petroselinum crispum*-assisted wet chemical route to synthesize $ZnFe_2O_4$ NPs. The SEM micrograph explains that the NPs' morphology and size depend on the synthesis environment (acidic or alkaline medium). Granular g rains of 250–400 nm size formed a pH = 2 medium; in contrast, agglomerated and lamellar NPs were created at pH = 9. Naik et al. [73] reported the synthesis of $ZnFe_2O_4$ NPs using (*Limonia acidissima*) wood apple juice as a reducing agent. Results indicated that the average crystallite size was 20 nm for spherical and agglomerate grains. The Ms, remanent magnetization (Mr), and Hc are 77.27 emu/g, 6.49 emu/g, and 898 Oe, respectively.

Ranganatha et al. [75] used *Aegle Marmelos* extract to fuel the preparation of $ZnFe_2O_4$ NPs (see Fig. 6-b). They demonstrated the average crystal size of NPs was 21 nm. In contrast, TEM images showed the formation of 50 nm $ZnFe_2O_4$ NPs with a significant effect of extract amount on the particles' shape, producing two different morphologies, spindle-like and sheet-like structures. The FTIR measurements confirmed the existence of a spinel structure by two bands at 407 and 528 cm^{-1} due to the lattice vibration in both A- and B- sites. Moreover, the observed Eg was about 2.36 eV. The Brunauer–Emmett–Teller (BET) analysis explains that $ZnFe_2O_4$ NPs have a 19.74 m^2/g surface area with a mesoporous nature, and the average pore size was 24 nm. The next generation of sustainable gas sensor applications can be built around these morphologies when coupled with green synthesis. Further, Sriramulu and their colleagues [76] used the *Aegle Marmelos* leaves extract with the co-precipitation route to prepare spinel $ZnFe_2O_4$ NPs. Spherical-shaped and agglomerated NPs (900 °C) were shown by SEM micrograph. This is due to the temperature calcination and duration strongly influencing the synthesis, size, and shape of the NPs [77]. The M–H loop confirmed a ferromagnetic nature with Ms and Hc of about 1.78 emu/g and 366 Oe.

T. Tatarchuk et al. [78] synthesized cobalt-doped $ZnFe_2O_4$ NPs through a honey-mediated sol-gel route. A 10–30 nm agglomerated and irregularly shaped NPs with sharp edges (see Fig. 8) were obtained. At the same time, the XRD findings recorded an increase in the average crystalline size from 14 nm to 18 nm with an increase in the Co ions up to 1. The same behavior was observed for magnetic parameters, including Ms and Hc. The Ms value increased from 10 to 69 emu/g, and the Hc from 48 to 1400 Oe. Indicated the significant effect of Co ions on the magnetic properties of $ZnFe_2O_4$ NPs.

N. Matinise et al. [24] decided to use a strong natural extract, *Moringa Oleifera,* to prepare non-stoichiometric $ZnFe_2O_4$ NPs via a wet chemical route. They demonstrate that the average crystalline size increased from 12.39 nm to 16.07 nm with increasing annealing temperature from 500 to 700 °C. Compared to the as-prepared sample, which has an amorphous nature. This behavior was observed again by HRTEM images, whereas the particle size increased from 5 nm to 25 nm with an increase in annealing temperature. And the nanograins have a non-regular, spherical-like, and agglomerated nature.

Piper nigrum (black pepper) seed extract was employed as a reducing/stabilizing agent by Din

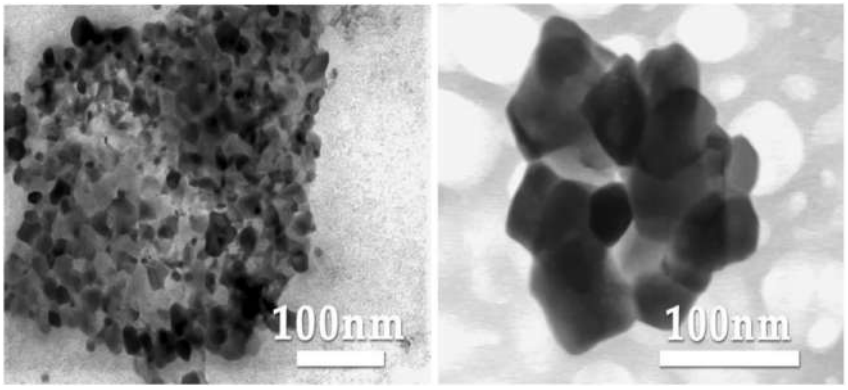

Fig. 8. TEM images of $ZnFe_2O_4$ NPs obtained from the green SGAC method according to [79].

et al. [18] to fabricate $ZnFe_2O_4$ NPs using a microwave-assisted hydrothermal method. The result indicated that $ZnFe_2O_4$ NPs have a particle size ranging between 60 and 80 nm and possessed a porous, rough morphology; however, the synthesized NPs tended to agglomerate. The phase nature of cubic spinel phase of the NPs was confirmed by XRD measurements. Furthermore, thermogravimetric analysis (TGA) indicated a maximum weight loss of approximately 32.61 % at 569.42 °C, likely attributed to the release of water molecules from the crystal structure of the $ZnFe_2O_4$ NPs.

Sugar cane juice assisted a sol-gel combustion route used to generate $ZnFe_2O_4$ NPs by Patil S.B and their colleagues [80]. They demonstrated that the calcination process enhances the crystalline nature of spinel $ZnFe_2O_4$ NPs with an average crystallite size of about 22.13 nm. The EDS and SEM analysis confirmed the existence of Zn, Fe, and O elements. And agglomerated spherical particles. Synthesized NPs display an Eg of about 2.2 eV, which is considered acceptable for photocatalysis applications. Aloe vera-assisted hydrothermal route to fabricate a series of spinel ferrite NPs in the form of AFe_2O_4, A = Zn, Mn, Ni, Mg, and Co. The SEM, XRD, and VSM measurements confirmed the plate-like structure of the nanocrystalline spinel phase with an average crystal size of 17.9 ± 3.1 nm, ~5–15 nm (SEM analysis), and a super-paramagnetic behavior with Ms value of 7.06 emu/g for $ZnFe_2O_4$ NPs [71]. Gavisiddaiah et al. [81] utilized Aloe vera extract to synthesize Cu-doped $ZnFe_2O_4$ NPs through a sol-gel auto-combustion route. The VSM loop demonstrated the soft ferromagnetic characteristics of the Cu-doped $ZnFe_2O_4$ NPs, with key magnetic parameters including Ms and Hc showing a decrease from 52.66 emu/g to 4.1 emu/g and 148 Oe to 112 Oe, respectively. This reduction is attributed to the diminished magnetic moment of Cu^{2+} ions as well as to the presence of the glassy state, surface effects, and surface spins. The highest and lowest dielectric constants and losses were recorded for $Zn_{0.5}Cu_{0.5}Fe_2O_4$ and $Zn_{0.7}Cu_{0.3}Fe_2O_4$ systems, respectively. The morphological and structural analysis revealed an increase in crystal size from 14.35 nm to 46.25 nm, while the lattice constant (a) decreased from 8.44 to 8.34 Å with a higher concentration of Cu^{2+} ions. SEM images indicated a notable transformation in the morphology of the NPs, transitioning from large clusters of multidimensional grains in pure $ZnFe_2O_4$ to uniformly distributed tiny spherical particles of Cu-doped $ZnFe_2O_4$, with a tendency for aggregation observed at high Cu^{+2} concentrations.

Pumpkin seeds (*Cucurbita moschata*) extract was used as a reducing agent to fabricate perylene decorated $ZnFe_2O_4$ NPs by Adawiah et al. [82]. The FTIR measurement indicated that the introduced $ZnFe_2O_4$ NPs did not damage the structure of the metal-organic frameworks (Cr-PTC MOF). Moreover, XRD confirmed the high crystallinity of $ZnFe_2O_4$ NPs compared with the low crystallinity of MOF Cr-PTC. The average crystal size ranged between 11.75 nm and 20.51 nm. The SEM images showed that the MOF Cr-PTC has cylindrical tube-like grains with varied lengths. In contrast, $ZnFe_2O_4$ NPs have relatively large chunk-shaped particles without any agglomeration (see Fig. 9). This is an advantage for the pumpkin seed extract, which produces a uniform shape and well-dispersed NPs, in opposite to other types of plant extract. A low Eg was recorded for $ZnFe_2O_4$ NPs and their nanocomposite of approximately 1.7 eV. This value makes the synthesized NPs/nanocomposites a good candidate for photo-catalyst applications. Further, the synthesis process used, aligned with the Green Chemistry principles, includes renewable feedstocks, producing safer materials, preventing waste, and using less energy.

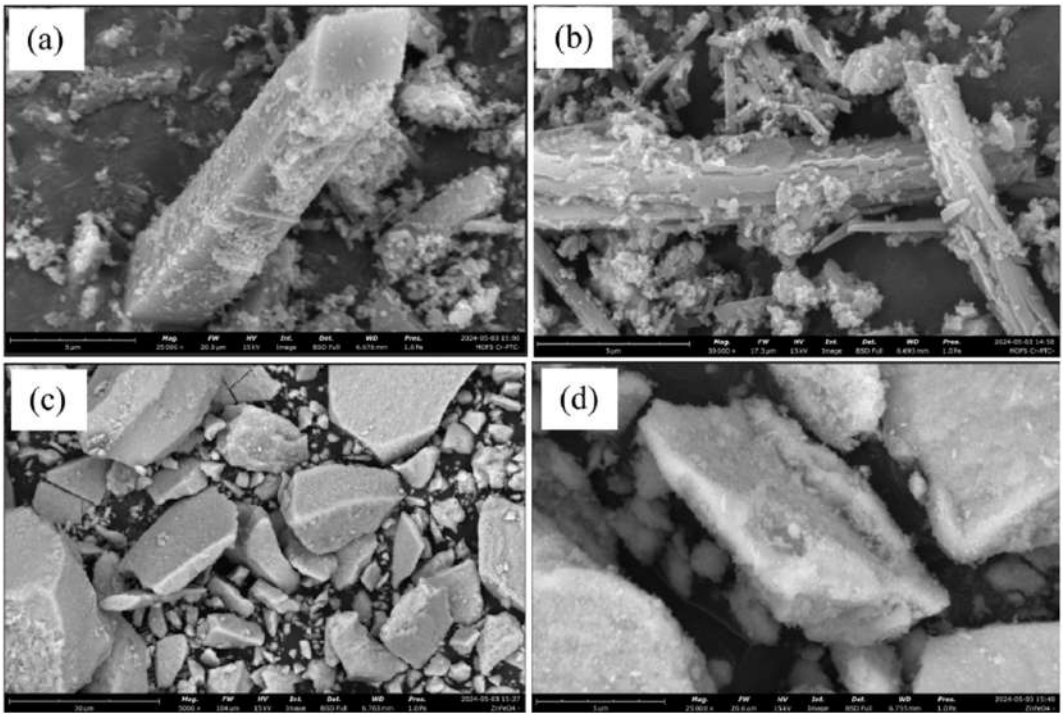

Fig. 9. The SEM micrograph of (a and b) Cr-PTC MOF, (c and d) $ZnFe_2O_4$ NPs [82].

N. Saridewi et al. [83] utilized (*Sansevieria trifasciata*) *Lidah mertua* extract (see Fig. 6-c) to fabricate $ZnFe_2O_4$ NPs through a hydrothermal route. Various extract amounts were used (1, 3, and 5 mL). Highly crystalline NPs were produced with different *Lidah mertua* amounts. Even a small amount, 1 mL of extract, can act as a capturing agent to synthesize $ZnFe_2O_4$ NPs. This is because of their phytochemicals and secondary metabolite compounds (hydroxyl groups). These compounds will stick to the crystal surface due to the electrostatic force between the surfaces, to inhibit the crystal growth rate and retain a uniform crystal shape [84]. The estimated crystal size was 30.54 nm, 26.15 nm, and 37.17 nm for $ZnFe_2O_4$ NPs prepared with 1 mL, 3 mL, and 5 mL of *Lidah mertua* extract. The smaller the crystal size, the larger the surface area, which increases its photocatalytic activity. Synthesized NPs have aggregate spherical particles with a 5–20 nm size distribution, which correlated with XRD results. The Eg of 3 mL $ZnFe_2O_4$ NPs was 1.8 eV, making it suitable for photocatalytic applications.

Both studies referenced above were conducted by Saridewi et al. and Adawiah et al., employed a highly concentrated reducing agent, NaOH, with a molarity of around 4 M during their NPs synthesis process. This choice of a strong chemical reducing agent significantly alters the traditional green synthesis method typically favored. The high concentration of NaOH may overshadow the beneficial effects of the naturally occurring phytochemicals normally involved in the synthesis, as it can replace these compounds and directly reduce metal ions such as Fe and Zn. Moreover, this methodology starkly contrasts the principles of Green Chemistry, which advocate for minimal use of resources and the avoidance of harmful by-products. By employing such an aggressive reducing agent, the process not only demands a larger quantity of starting materials but also generates unwanted by-products that undermine the sustainability and environmental friendliness of the synthesis. Fig. 10 shows the roadmap of the green synthesis of $ZnFe_2O_4$ NPs.

$Zn_{0.4}Ni_{0.35}Cu_{0.25}Fe_2O_4$ NPs were prepared utilizing *tragacanth* gum as a bio-route assisted sol-gel route by Fardood et al. [85]. The $Zn_{0.4}Ni_{0.35}Cu_{0.25}Fe_2O_4$ NPs exhibit a ferromagnetic nature with Ms of about 52.76 emu/g and Hc of 80.14 Oe. The two main bands related to the M–O vibration in the octahedral (B-site) and tetrahedral (A-site) were observed at 430 cm^{-1} and 580 cm^{-1}. A narrow size distribution of uniform, aggregated spherical NPs with an average crystalline size of ~20 nm was achieved.

For the first time, Najm et al. [86] used *Eucalyptus* leaf extract as reducing and capping agents to synthesize $ZnFe_2O_4$ NPs through a microwave-

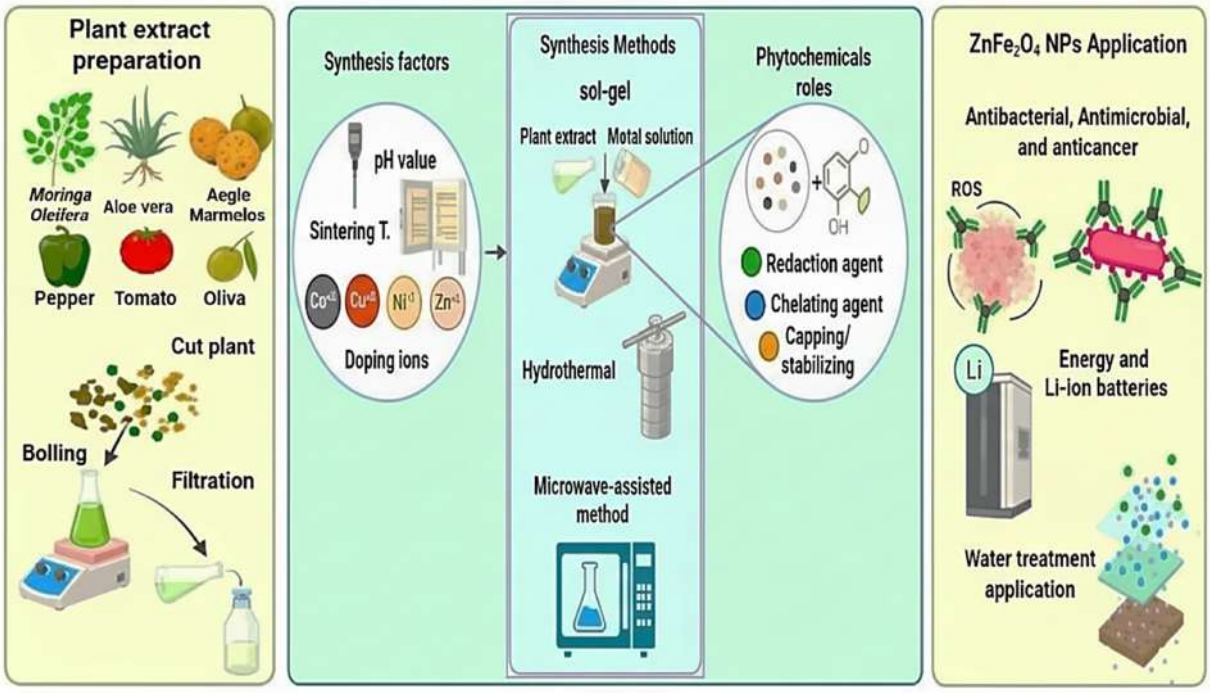

Fig. 10. Shows the roadmap of the green synthesis of $ZnFe_2O_4$ NPs.

assisted wet chemical process. The observed Eg was 2.52 eV, higher than other researchers' values. The FTIR spectrum confirms the presence of metal-oxygen (M−O) bonds, showing a weak band at 441.70 cm^{-1} and a stronger band at 551.64 cm^{-1}, corresponding to the A- and B- sites of the $ZnFe_2O_4$ spinel phase. EDS analysis verified the presence of Zn, Fe, and O elements without contamination. SEM images showed the formation of homogeneous, well-distributed, and agglomerated NPs. A high negative Zeta potential value of - 47.41 mV indicates good stability of the $ZnFe_2O_4$ NPs, attributed to phenolic compounds in *Eucalyptus* leaf extract. Structural studies revealed the formation of two phases: spinel $ZnFe_2O_4$ and hematite (-Fe_2O_3) NPs. Table 2 summarizes the possible role of the phytochemical in the plant extract in the synthesis process of $ZnFe_2O_4$ NPs [87–90]. Further, Table 3 represents a comparison of plant-mediated $ZnFe_2O_4$ NPs synthesis.

All plant extracts used to synthesize $ZnFe_2O_4$ NPs, which were mentioned above, contain various phytochemicals such as polyphenols, flavonoids, terpenoids, reducing sugars, steroids, lignans, carbohydrates, and organic acids that act as reducing, capping, chelating, and stabilizing agents. Further, the synthesis method, doping ions, sintering/ annealing temperature, pH value, and plant extract amount affect the structural, morphological, optical, and magnetic properties of the synthesized $ZnFe_2O_4$ NPs. For instance, using different types of plant extracts yielded varying characteristics for

Table 2. Represents the possible phytochemical role in the synthesis of $ZnFe_2O_4$ NPs.

Natural Sources (Extracts)	Phytochemical Group	Primary Roles in NP Synthesis
Lawsonia inermis, Piper nigrum, Moringa oleifera	Polyphenols	Effective reducing agents for Fe^{3+} and Zn^{2+} ions stabilize nuclei through chelation.
Eucalyptus leaves, Pumpkin seeds, Limonia acidissima	Terpenoids	Capping and growth-direction agents help with nucleation and control the shape of NPs.
Hibiscus rosa-sinensis, Opuntia dillenii haw	Alkaloids	Minimize the presence of ionic species to help stabilize and disperse NPs.
Sugarcane juice, Honey, Tragacanth gum	Carbohydrates/Sugars	Act as both reducing and capping agents to enhance colloidal stability.
Citrus, Honey, Tragacanth gum	Organic acids	Strong chelating agents, pH regulators, and control particle size
Pumpkin seeds, Moringa	Steroids/Lignans	Hydrophobic barriers help in phase stability and aggregation resistance

Table 3. A comparison of Plant-Mediated $ZnFe_2O_4$ NPs Synthesis.

Synthesis Method	Extract Type	Crystalline Size (nm)	Magnetic Properties (Ms/Hc)	Doping Ions	Work Year	Ref.
Sol-gel	*Aloe vera*	15–70	Not specified	None	2011	[68]
Microwave/Conventional combustion	*Hibiscus rosa-sinensis*	39 (MCM), 81 (CCM)	63.61–255.7 memu/g	None	2016	[21]
Microwave/Conventional combustion	*Opuntia dillenii haw*	32–73	47.13–1024 memu/g	None	2017	[70]
Sol-gel	*Tragacanth gum*	~20	52.76 emu/g, 80.14 Oe	Ni^{2+}, Cu^{2+}	2017	[85]
Co-precipitation	*Aegle marmelos*	Not specified	1.78 emu/g, 366 Oe	None	2018	[76]
Wet chemical	*Moringa oleifera*	12.39–16.07	Not specified	None	2018	[24]
Sol-gel combustion	*Sugarcane juice*	22.13	Not specified	None	2018	[80]
Wet chemical	*Petroselinum crispum*	250–400 (pH 2), lamellar (pH 9) SEM	Not specified	None	2019	[74]
Microwave-assisted	*Limonia acidissima*	20	77.27 emu/g, 6.49 emu/g, 898 Oe	None	2019	[73]
Sol-gel	*Lawsonia inermis*	17.12	42.9 emu/g, 11.9 Oe	None	2020	[69]
Sol-gel	*Aegle marmelos*	21 (XRD), 50 (TEM)	Not specified	None	2020	[75]
Microwave-assisted hydrothermal	*Piper nigrum*	60–80	Not specified	None	2020	[17]
Sol-gel	*Honey + Citric acid*	14–18	10–69 emu/g 48 - 1400 Oe	Co^{2+}	2021	[78]
Sol-gel	*Aloe vera*	14.35–46.25	52.66 to 4.1 emu/g, 148 to 112 Oe	Cu^{2+}	2022	[91]
Hydrothermal	*Lidah mertua*	26.15–37.17	Not specified	None	2024	[83]
Sol-gel	*Pumpkin seeds*	11.75–20.51	Not specified	None	2025	[82]
Microwave-assisted wet chemical	*Eucalyptus leaves*	Not specified	Not specified	None	2025	[86]

$ZnFe_2O_4$ NPs. Where the crystalline size varied between 11.75 nm (Pumpkin seeds, sol-gel route) to 81 nm (*Hibiscus rosa-sinensis*, CCM), Eg varied between 1.7 eV (Pumpkin seeds, sol-gel route) to 2.52 eV (*Eucalyptus leaves*, Microwave-assisted wet chemical method), Ms value changed from 47.13 memu/g (*Opuntia dillenii haw,* CCM) to 77.27 emu/g (*Limonia acidissima,* microwave-assisted method). Therefore, we can conclude that the most significant factors affecting the characteristics of $ZnFe_2O_4$ NPs are plant extract type and synthesis route. The sol-gel route is more frequently used for the green synthesis of NPs, afterwards microwave and conventional combustion methods. Therefore, the synthesized NPs have a narrow crystalline size distribution of ~10–80 nm. And this narrow particle size distribution affects their physicochemical properties, such as optical and magnetic qualities.

Comparatively, *Aegle marmelos* extract creates optimal crystalline size of $ZnFe_2O_4$ NPs ~21 nm, mesoporous morphology (BET = 19.74 m^2 g^{-1}), and moderate Eg = 2.36. Which very recommended for photocatalytic and gas-sensing applications. The combination of the sol-gel route and *Aegle marmelos* extract provides the required balance to synthesize NPs with excellent properties make it a good choice for advanced applications. This balance came from the active phytochemical exist in *Aegle marmelos* extract and the advantages of the cost-effective sol-gel route. Furthermore, Pumpkin seeds can be another excellent choice in combination with the sol-gel route for synthesizing $ZnFe_2O_4$ NPs with balanced physicochemical qualities (D = 11.75–20.51 nm, Well-dispersed; chunk-like particles, and Eg ~ 1.7 eV) demonstrate a good photocatalytic activity against malachite green (MG) (~81.13 % in 30 min at pH = 6, 0.5 g/L catalyst). In contrast, *Hibiscus rosa-sinensis*, *petroselinum crispum,* and *Opuntia dilenii haw* extracts yielded higher crystalline size (32 nm–81 nm), larger particle size distribution, several hundred nanometers, and noticeable aggregation, leading to a significant reduction in Ms value 63.61–255.7 memu/g (*Hibiscus rosa-sinensis*), 47.13–1024 memu/g (*Opuntia dillenii haw*). Indicated the adverse impact of these extracts on the qualities of the $ZnFe_2O_4$ NPs.

10. Applications of $ZnFe_2O_4$ NPs synthesized through plant-mediated method

Anticancer & antimicrobial activity: Biocompatibility refers to NPs' ability to react safely with biological systems without causing adverse effects such as cytotoxicity, genotoxicity, immunotoxicity, irritation, sensitization, and hemocompatibility.

$ZnFe_2O_4$ NPs demonstrated a strong biocompatibility because the low toxicity of Fe^{+3} and Zn^{+2} ions, which provide safe use in biomedical domains by matching human daily intake limitations compared to other metallic materials [92]. Further, the green synthesis of $ZnFe_2O_4$ NPs provides an additional feature that enhances biocompatibility due to natural reducing and capping agents from plant extracts, which lessen cytotoxicity, provide safer surface chemistry, and enhance stability in biological systems, positively influencing their biomedical utility [93].

Strong antitumor effects of $ZnFe_2O_4$ NPs on breast cancer cell lines (MCF-7) were observed by Sarala [69]. $ZnFe_2O_4$ NPs were used with doses of 25, 50, 100, 250, and 500 g/mL; cell viability dropped dramatically by 60 %, 53 %, 44 %, 32 %, and 24 %, respectively. These findings can be described by generating reactive oxygen species (ROS). This is due to its Fe-based NPs, and introducing any Fe-based NPs affects the bacteria's iron metabolism system [94,95]. When $ZnFe_2O_4$ NPs come into direct contact with cell walls, the membrane is deformed and ruptured, ROS are produced on the $ZnFe_2O_4$ NPs surface, and the particles dissolve and release free Zn^{2+} ions, which causes ROS to be produced inside the cells [69,96].

Generally, the mechanism of antibacterial activity in $ZnFe_2O_4$ NPs can be due to metal ion release, reactive oxygen species (ROS), oxidative stress, and physical damage. When the NPs are adherent to the bacterial surface due to electrostatic interactions between them. The rough surface of NPs (especially with sharp edge morphologies) caused a disruption and pit formation in the cells' lipid bilayer. Results in leakage of intracellular contents such as cytoplasm and proteins. Moreover, the mobility and penetration of $ZnFe_2O_4$ NPs can be increased in the presence of alternating magnetic fields [97]. Notably, this mechanism frequently appeared with Gram-negative bacteria such as *E. coli, P. aeruginosa, K. pneumonia*, etc., because their thinner peptidoglycan layer and high electrostatic attraction due to lipopolysaccharide-rich outer membrane [98].

$ZnFe_2O_4$ NPs can generate ROS such as hydroxyl radicals ($OH^{\bullet}$), superoxide anions ($O_2^{\bullet -}$), and hydrogen peroxide (H_2O_2) by surface redox cycling and Fenton-like reactions. The partially inverse or normal spinel structure of $ZnFe_2O_4$ NPs possesses a redox reaction of Fe^{+3}/Fe^{+2} ions combined with a high surface area of NPs amplifying the effect of the surface Fe ions, which reduces molecular oxygen (O_2) to superoxide radicals ($O_2^{\bullet -}$). Further, Fenton-like reaction generates hydroxyl radicals ($OH^{\bullet}$) and hydroxyl anions (OH^-). After NPs adhere, the released ROS build up at the bacterial interface and cause severe oxidative stress that results in lipid peroxidation, protein oxidation, and DNA damage. Bacterial antioxidant defences are overwhelmed by the non-selective and catalytic nature of Fenton-driven ROS generation, which causes permanent membrane rupture and cell death [99,100] Lastly, $ZnFe_2O_4$ NPs show a slow dissolution in physiological or acidic microenvironments, releasing Zn^{2+} and Fe^{3+} ions. These ions bind to bacterial enzymes and DNA and inhibit the main metabolic and replication processes. Even at low NPs concentrations, metal ion release collaborates with ROS to raise bacterial death.

Different pathogenic bacterial strains, including *Staphylococcus aureus*, *Escherichia coli*, *Pseudomonas desmolyticum*, and *Klebsiella aerogenes,* were used to evaluate the antibacterial activity of microwave-assisted *Limonia acidissima* juice-synthesized $ZnFe_2O_4$ NPs. At different doses, 50, 100, and 150 g/ L. The results showed that the zone of inhibition (ZOI) ranged between 2.63 and 8.83 mm, 2–10.5 mm, 2.83–7.33 mm, and 1.5–7.5 mm for *S. aureus*, *E. coli, P. desmolyticum, and K. aerogenes,* respectively. Also, findings indicated a significantly higher antibacterial activity in *S. aureus*, *E. coli,* and *P. desmolyticum*. While *K. aerogenes* shows moderate activity compared to *E. coli* and *S. aureus* [73]. As previously mentioned, the antibacterial activity of NPs is influenced by the production of ROS, which is in turn affected by factors such as shape, size, and specific surface area of the NPs. In this study, the authors highlighted the effective antibacterial properties of $ZnFe_2O_4$ NPs, attributing this to the strong interaction between the rough corners and sharp edges of the synthesized NPs and the bacterial cell membrane. This interaction ultimately resulted in damage to the bacteria's DNA replication processes, leading to cell death due to protein denaturation.

A. Omelyanchik et al. indicated that magnetic ferrite NPs with the formula MFe_2O_4, where $M = Zn^{2+}$ and Co^{2+}, have significantly inhibited the growth of *Escherichia coli* K-12 MG1655. At the same time, the optical density (OD_{600}) showed a decrease in bacterial concentration in treated cultures compared to the control. Furthermore, a good antibacterial activity was observed for $ZnFe_2O_4$ and $CoFe_2O_4$ due to their strong inhibition results.
B. *subtilis, E. coli, S. aureus,* and *P. aeruginosa* bacterial strains were tested using $ZnFe_2O_4$ NPs synthesized via a sugar cane juice extract. The ZOI measurements for the

mentioned strains were observed at 15.5 mm, 9 mm, 11.5 mm, and 9.5 mm, respectively, which are lower than the control (Ciprofloxacin). This is attributed to two main factors: firstly, zinc tends to interact with microbial membranes, which leads to prolonged cell division. Secondly, due to its large surface area and active oxides. $ZnFe_2O_4$ NPs may penetrate deeply and compromise bacterial cell walls. Additionally, the authors did not provide a thorough analysis of the morphological characteristics that could have influenced the antibacterial efficacy.

The same bacterial strains mentioned above were used to examine the antibacterial activity of *Aegle marmelos* mediated $ZnFe_2O_4$ NPs [76]. The ZOI was detected as follows: *Bacillus subtilis*, 23 mm; *E. coli*, 17 mm; *P. aeruginosa*, 25 mm; and *S. aureus*, 22 mm, which yields a better ZOI and, consequently, better antibacterial activity. Moreover, the synthesized NPs exhibit a promising carfilzomib drug release. In approximately neutral medium (pH = 7.4), $ZnFe_2O_4$ NPs successfully released 95 % of the carfilzomib drug after 6 h. This is a fast release compared with other works by [101,102].

A huge study reported by Ranganatha et al. [75], where they used eight bacterial and four fungal strains to evaluate the antimicrobial activity of $ZnFe_2O_4$ NPs synthesis by *Aegle Marmelos* extract with various amounts (2.5, 5, 7.5, and 10 mL). The used strains are *S. aureus, S. aureus (MRSA), E. aerogenes, M. luteus, K. pneumonia, S. typhimurium, S. paratyphi-B, P. vulgaris, C. albicans, B. cinerea, M. pachydermatis, and C. krusei*. We can conclude several points from this study. First, all samples display a good antimicrobial activity against the mentioned strain according to the ZOI test. Second, the samples prepared with a high *Aegle Marmelos* amount exhibited a minimum ZOI against all microorganism strains. Third, 2.5 mL-$ZnFe_2O_4$ NPs have the highest ZOI. Lastly, the variation in the ZOI was as follows: 18–14 mm, 15–9 mm, 18–11 mm, 19–14 mm, 14–12 mm, 20–13 mm, 12–9 mm, and 17–11 mm for *S. aureus, S. aureus (MRSA), E. aerogenes, M. luteus, K. pneumonia, S. typhimurium, S. paratyphi-B, P. vulgaris, C. albicans, B. cinerea, M. pachydermatis, and C. krusei,* respectively. Imraish et al. [103] studied the anticancer activity of $ZnFe_2O_4$ NPs prepared via *Boswellia carteri* extract against various cancer cell lines, including MDA-MB-231, K562, and MCF-7, in addition to normal fibroblasts. The results confirmed that the green synthesis $ZnFe_2O_4$ NPs have an average crystal size of 10.54 nm. MTT cytotoxicity assay demonstrated a selective and potent anticancer activity against K562 and MDA-MB-231 cell lines with IC50 values of 4.53 M and 4.19 M, respectively. With minimal adverse side effects on normal cells.

In conclusion, the biocompatible, green-synthesized $ZnFe_2O_4$ NPs provide a better characteristic compared to chemically fabricated NPs. Utilizing plant extract phytochemicals as reducing and capping agents yields NPs with cleaner surface chemistry, minimal residual toxicity, and safer interactions with cells, tissues, and antimicrobial systems. Consequently, green-synthesized $ZnFe_2O_4$ NPs possess strong potential for use in antimicrobial and anticancer applications, drug delivery, wound healing, and magnetic resonance imaging contrast agents.

Ion-lithium batteries: The impressive electrochemical properties of $ZnFe_2O_4$ NPs make them an excellent choice for use as an anode electrode in lithium-ion batteries. Cyclic voltammetry (CV) and electrochemical impedance spectroscopy (EIS) tests were conducted on a $ZnFe_2O_4$-modified glassy carbon electrode nanocomposite synthesized using a green *Moringa Oleifera* extract for electrochemical applications. The results revealed that the $ZnFe_2O_4$ NPs demonstrated low charge-transfer resistance and robust redox behavior. A low time constant of 5.2×10^{-4} s/rad and a high exchange current of 6.59×10^{-4} A cm^{-2} suggest rapid electron transfer kinetics and efficient interfacial conductivity. The findings establish the nanocomposite as a promising electrode material for lithium-ion batteries and other advanced electrochemical energy storage systems [24]. Another study by Ranganatha et al. [75] demonstrated that the synthesis of $ZnFe_2O_4$ NPs using varying amounts of *Aegle Marmelos* extracts yields a significantly enhanced current response in CV analysis. This suggests that $ZnFe_2O_4$ NPs efficiently promote electron diffusion between the electrode surface and the electrolyte. The quick and great electrochemical reversibility of the redox process reaction is highlighted by the oxidation and reduction peaks, which are discernible within the potential range of −0.6 to 1.5 V across all scan rates of 10–50 mV/s.

Catalyst activity: Kombaiah et al. [70] used various amounts of $ZnFe_2O_4$ NPs as a catalyst, ranging from 0 to 0.09 g, to generate formic acid and glycolic acid. The results demonstrated that the highest glycerol conversion rates, 97 % in MHM and 84 % in CHM, and the maximum selectivity for formic acid, 99 % in MHM and 86 % in CHM, were achieved with the use of 0.05 g of catalyst for the selective oxidation of glycerol to formic acid. This indicates that the catalyst exhibits strong catalytic

performance and enhanced selectivity for formic acid throughout the reaction.

The catalyst activity of $Zn_{0.4}Ni_{0.35}Cu_{0.25}Fe_2O_4$ NPs, synthesized using *tragacanth* gum, was enhanced for the production of polyhydroquinoline derivatives under microwave irradiation in solvent-free conditions. The highest recorded activity was 97 %, which decreased to 92 % after six cycles. This performance surpasses that reported in other studies utilizing conventional methods for synthesizing Zn-ferrite NPs. This finding underscores the effectiveness of an inexpensive, non-toxic, and straightforward green synthesis route that promotes the growth of ferrite NPs (e.g., $ZnFe_2O_4$ NPs) with excellent properties, making them a preferred choice for advanced applications.

Water Treatments: The future quality of drinking water for generations to come is significantly threatened by the pervasive pollution of our water resources. This contamination arises from the substantial release of various harmful substances, including dyes, organic chemical compounds, and pharmaceutical residues. These pollutants are by-products of numerous industrial sectors, such as pharmaceuticals, cosmetics, petrochemicals, and textiles, all of which contribute to the degradation of our freshwater sources. As these industries continue to operate, they release these toxic materials into the environment, endangering the health and safety of our water supplies [104,105] Dyes such as Evans blue (EB), methylene blue (MB), Rose Bengal (Rb), malachite green (MG), etc., a toxic-pollutants that can cause sickness, nausea, cyanosis, mental disorientation, elevated heart rate, jaundice, tissue necrosis, and methemoglobinemia issues when consumed orally. And their photocatalytic breakdown is very significant to eliminate them [106,107]. The photocatalytic activity of $ZnFe_2O_4$ NPs was recorded against EB and MB dyes by Naika et al. [73]. The results showed that in 90 min, the absorbance of MB and EB had drastically dropped, yielding 89 % and 99.66 % degradation, respectively.

$ZnFe_2O_4$ NPs synthesized using *Piper nigrum* (black pepper) extract demonstrated outstanding photocatalytic performance in the degradation of MB dye, as reported by Din et al. [18]. Their findings indicated that the UV−Visible spectra of MB showed a time-dependent decolorization, with complete elimination of the dye achieved after 90 min of treatment with $ZnFe_2O_4$ NPs.

MB and Rb dyes were used to evaluate the photocatalytic activity of $ZnFe_2O_4$ NPs prepared by sugarcane juice extract [80]. The results demonstrated that the photocatalytic activity of mixed and individual dyes showed a time-dependent performance, with complete elimination of the dye achieved after 150 min of treatment with $ZnFe_2O_4$ NPs. Moreover, an alkaline medium exhibits better photocatalytic activity than an acidic medium. Further, the best photocatalytic activity of $ZnFe_2O_4$ NPs was observed at 50 mg, over other doses ranged between 25 and 100 mg. The $ZnFe_2O_4$ NPs maintain the same crystal phase, morphology, and photocatalytic activity after four degradation cycles.

MG dye was targeted by $ZnFe_2O_4$ NPs and Cr-PTC/$ZnFe_2O_4$ nanocomposites synthesized by Pumpkin seeds (*Cucurbita moschata*) extract. PTC/$ZnFe_2O_4$ nanocomposites (1:1) exhibited the highest degradation performance of 81.13 % at a MG dose of 40 mg/L, a pH value of about 6, a catalyst dosage of 0.5 g/L, and an irradiation time of 30 min [82]. A photocatalyst's capacity to degrade will typically diminish as the dye concentration rises. The substance MG has the properties of a light absorber, much like MB. The light intensity that may enter and penetrate the photocatalyst decreases as the concentration of MG in the solution increases. It makes the photocatalyst not exposed to light. It makes it difficult for the electron excitation process to take place by preventing the light energy that enters the solution system from penetrating and striking the photocatalyst surface. This leads to the suppression of the production of superoxide radicals ($O\cdot^{2-}$) and hydroxyl radicals ($\cdot OH$), which contribute to the breakdown of MG [82,91].

A significant degradation of MB was achieved by Saridewi and their team [47], who employed $ZnFe_2O_4$ NPs as the degradation agent (see Fig. 11). They reported photocatalytic activities of 95.1 %, 98.41 %, and 93.51 % with varying amounts of *Lidah mertua* after 120 min. Notably, the prepared 3 mL $ZnFe_2O_4$ sample exhibited the highest photocatalytic performance against MB dye. Additionally, the alkaline medium (pH = 9 and 12) demonstrated superior photo-degradation efficiency compared to the acidic medium (pH = 6). It was also observed that the photocatalytic efficiency declined by approximately 77 % as the concentration of MB increased from 20 ppm to 40 ppm. Lastly, $ZnFe_2O_4$ NPs can be utilized for up to four reaction cycles, with degradation efficiency ranging from 95.33 % to 76.95 %.

$ZnFe_2O_4$ NPs synthesized using *Eucalyptus* leaves extract were employed to explore the degradation of acid black 210 (AB210) dyes. The findings indicated removal efficiency compared to the adsorption method, with photocatalytic degradation occurring at a faster rate than adsorption. Notably, a complete removal efficiency of 100 % was

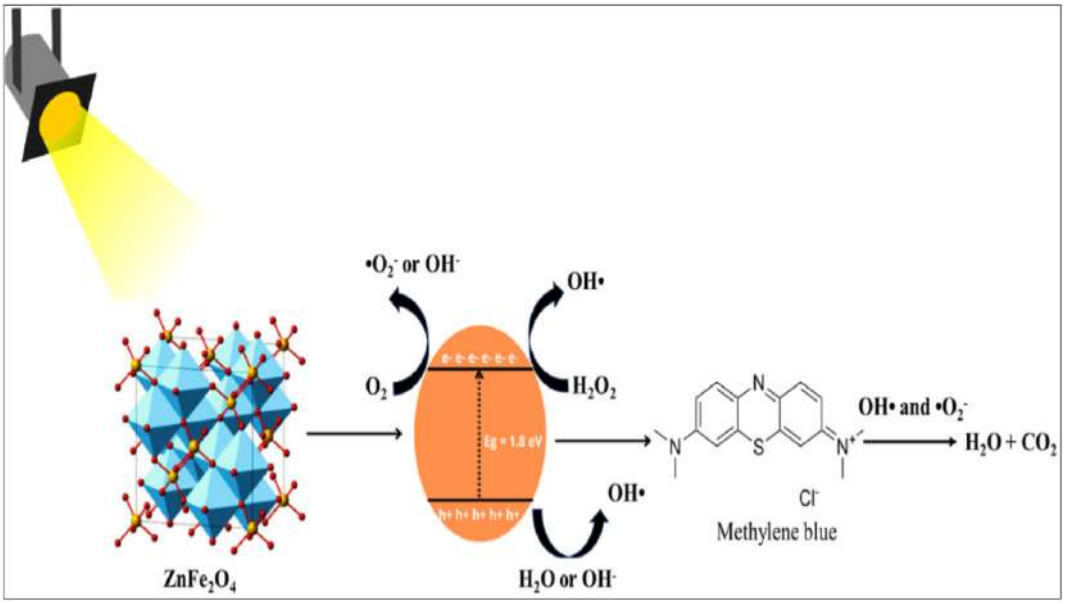

Fig. 11. The photo-degradation mechanism of dyes by $ZnFe_2O_4$ NPs [83].

achieved at a concentration of 5 mg/L of AB210 within just 30 min, under optimal conditions of pH 7, UV intensity of 24 W/m^2, and a temperature of 45 °C [86]. Ranganatha et al. tested the photo-degradation of MB by *Aegle Marmelos* fuel synthesis $ZnFe_2O_4$ NPs. They carried out their test with various parameters, such as dye concentration and NPs doses. The results show a dye concentration-dependent activity of NPs and reach a peak value after 120 min. Furthermore, $ZnFe_2O_4$ NPs with a 10 mg dose exhibited better photo-degradation performance than other doses ranging between 20, 30, and 40 mg. This reduction is due to agglomeration and sedimentation of the catalyst. Moreover, the pH has an important role in the photo-degradation of the MB dye. Where the pH level varied between 3 and 11, with variation in degradation between 75 % and 95 %. Reusability of synthesized NPs shows that after 5 cycles XRD pattern appears the same as a fresh catalyst, there is no change in intensities of the peaks [75]. This shows that the catalyst can be reused for several photo-degradation processes under visible light. And the catalyst activity remained above 85 %. Table 4 summarizes a comparison of plant-mediated $ZnFe_2O_4$ NPs applications in various fields.

11. Conclusion and challenges

The green synthesis of $ZnFe_2O_4$ NPs using plant-mediated routes is a promising and sustainable alternative to conventional physical and chemical methods. These routes use green feedstocks, eliminate the need for hazardous reagents, prevent the generation of harmful by-products, and minimize energy consumption by combining plant extracts with microwave and/or ultrasonic approaches. In comparison, synthesis methods for NPs fabricated via plant extracts, such as *Aloe vera, Hibiscus rosa-sinensis, Eucalyptus leaves, and Moringa oleifera,* yield desirable physicochemical properties, including superparamagnetism, narrow band gaps, high surface area, and varied magnetic characteristics. Furthermore, these biogenic $ZnFe_2O_4$ NPs have demonstrated significant potential across a spectrum of advanced applications, including efficient photocatalytic degradation of organic pollutants, strong antibacterial and anticancer activities, and excellent electrochemical performance in lithium-ion battery systems. However, challenges remain in standardizing plant-based protocols and scaling up synthesis for industrial applications. Future research should focus on mechanistic understanding, reproducibility, and hybridization with other functional materials to enhance performance and applicability. Overall, plant-mediated $ZnFe_2O_4$ NPs represent a versatile and sustainable nanoplatform for next-generation green technologies. Therefore, the main challenges can be listed:

1. One of the major challenges facing the green synthesis strategies is the phase purity of the synthesis NPs, where achieving phase-pure $ZnFe_2O_4$ using green synthesis may be complex process. Due to various factors, including the type of phytochemical existing in plant extracts,

Table 4. A comparison of Plant-Mediated $ZnFe_2O_4$ NPs Applications.

Extract Type	NPs Properties	Band Gap (eV)	Degradation Efficiency	Applications	Work Year	Ref.
Aloe vera	Polycrystalline, spinel structure, agglomerated NPs	Not specified	Not specified	Photocatalysis, magnetic applications	2011	[68]
Hibiscus rosa-sinensis	Rough, agglomerated NPs	Not specified	Not specified	Magnetism, morphology control	2016	[21]
Opuntia dillenii haw	Agglomerated grains; Ms = 47.13−1024 memu/g	Not specified	Not specified	Glycerol oxidation catalysis	2017	[70]
Tragacanth gum	Spherical, uniform; Ms = 52.76 emu/g; Hc = 80.14 Oe	Not specified	97 % yield of polyhydroquinolines (organic catalysis)	Microwave-assisted catalysis (organic synthesis)	2017	[85]
Moringa oleifera	Spherical, non-uniform, amorphous to crystalline	Not specified	Not specified	Lithium-ion battery (anode), electrochemistry	2018	[24]
Sugarcane juice	Spherical, agglomerated NPs	2.2	98.41 % (RB) in 150 min	Mixed dye photodegradation, antibacterial	2018	[80]
Petroselinum crispum	Lamellar/sheet-like (alkaline)	Not specified	Seed germination inhibition 100 % at 10^{-3} M (acidic $ZnFe_2O_4$)	Toxicological bioassays	2019	[74]
Limonia acidissima	Spherical, agglomerated NPs, Ms = 77.27 emu/g, Hc = 898 Oe	Not specified	99.66 % (EB) & 89 % (MB) in 90 min	Photocatalysis, antibacterial	2019	[73]
Lawsonia inermis	Homogeneous, agglomerated NPs, Ms = 42.9 emu/g, Hc = 11.9 Oe	Not specified	Anticancer inhibition 76 % at 500 g/mL	Breast cancer inhibition (MCF-7), antibacterial	2020	[69]
Aegle marmelos	Spindle/sheet; BET = 19.74 m^2/g; mesoporous	2.36	~95 % carfilzomib release (6 h); strong antibacterial ZOI up to 25 mm	Drug delivery, antibacterial, photocatalysis	2020	[75]
Piper nigrum	Porous, rough, spinel + secondary phase	Not specified	100 % (MB) in 90 min	Photocatalytic dye degradation	2020	[17]
Citric acid	Irregular, sharp; Co-doped; Ms = 10−69 emu/g	Not specified	Not specified	Hyperthermia, Pb^{2+} adsorption	2021	[78]
Aloe vera (Cu-doped)	Cu^{2+} doping reduced Ms from 52.66 to 4.1 emu/g	Not specified	Not specified	Dielectrics, catalysis, magnetic devices	2022	[91]
Lidah mertua	Spherical aggregates (5−20 nm); extract dose-dependent size	1.8	Up to 98.41 % (MB) in 120 min (best at 3 mL extract); reusable for four cycles	Photocatalysis (MB), extract optimization	2024	[83]
Pumpkin seeds	Well-dispersed; chunk-like	~1.7	81.13 % (MG) in 30 min at pH = 6, 0.5 g/L catalyst	Photocatalysis (malachite green), nanocomposite stabilization	2025	[82]
Eucalyptus leaves	Mixed $ZnFe_2O_4$ + -Fe_2O_3 phases, good dispersion; zeta = −47.41 mV	2.52	100 % removal of acid black 210 in 30 min at 5 mg/L	Fast photocatalysis, stable aqueous dispersions	2025	[86]

their activity in reducing and stabilizing the generated NPs, in other words, the active functional groups in the phytochemical and its effectiveness, amount of the plant extracts used in the synthesis process, synthesis method, and other synthesis parameters (e.g., pH value, temperature, pressure, etc.).
2. Although several studies suggest that the plant extract phytochemicals, such as flavonoids, terpenoids, phenolic acids, etc., significantly act as reducing, capping, and stabilizing agents in the synthesis of ferrite NPs. There are incomplete and limited understanding of the specific role of each bio-component in the nucleation control, particle growth, and morphology, and surface chemistry. Causing issues in the reproducibility process.
3. The variability of natural extracts is due to species, geographic origin, seasonal effects, and extraction method. This leads to inconsistent NPs characteristics (altering crystal structure, morphology, optical qualities (e.g., energy bandgap), and magnetic properties (e.g., Ms, Hc, etc.). Increasing the difficulties in the cross-study comparability and standardization.
4. Green synthesis of $ZnFe_2O_4$ NPs displays remarkable properties, such as small size, large surface-to-volume area, and higher reactivity. Possess both positive and negative effects depending on how it interacts with ecosystems and biological systems. Furthermore, the limited number of in vivo biocompatibility studies and the inadequate understanding of toxicological and environmental effects restrict safe usage.
5. The requirements for optimized synthesis parameters (e.g., size distribution, cation/anion arrangement, and morphology control), efficient yield improvement, and reliable transfer of lab-scale protocols to industrial-scale production.

12. Future directions

Based on the main challenges faced by the synthesized $ZnFe_2O_4$ NPs, we suggest that future research projects should be focused on one of the following directions:

1. Future studies should focus on prioritizing molecular-level studies that clarify how specific bio-components, such as reduction, chelating, capping, nucleation, and stabilization of $ZnFe_2O_4$ NPs.
2. Developing standardized and scalable protocols for extract preparation and reaction conditions.
3. Diversifying sources of extracted materials and exploring available plant extracts, such as algae [108]. Moreover, expanded the use of other biosources such as bacteria, fungi, and biowaste.
4. Integrating green synthesis with advanced methods (microwave, ultrasound, hydrothermal) to enhance efficiency and energy savings. In addition to integrating the doping strategy to overcome the performance limitations in photocatalysis applications, as well as developing the performance in biomedical applications.
5. Conducting systematic life-cycle and cost-effectiveness analyses.
6. Explore the possibility of using $ZnFe_2O_4$ NPs in other promising applications, such as bone regenerative medicine. Studies show that metal oxide NPs, which have been demonstrated to accelerate bone repair and have a beneficial impact on mesenchymal stem cells in addition to their antibacterial and anti-inflammatory properties, can assist in improving bone healing [109].
7. Used Artificial intelligence (AI) and machine learning (ML) to build models that can predict the best synthesis methods besides other synthesis parameters such as extract amount, pH level, temperature, annealing/sintering temperatures and duration, etc., to obtain the desirable properties of NPs. Based on a huge number of research articles for creating these models.

Source of Funding

There is no funding.

Conflict of Interest

There are no conflicts of interest to disclose.

Ethical Approval

The study was conducted in accordance with ethical standards. This research does not involve experiments on humans or animals.

Data Availability

All relevant data are included within the review.

Author Contributions

Rihab Jabbar: Writing - Original Draft. Review and Editing.

References

[1] Khanahmad A, Ebrahimi Z, Abreshteh A, Pajavand H, Satarzadeh N, Dousari AS. Biological applications of nanoparticles synthesized via Olea europaea plant: a comprehensive review. Int J Polym Sci Jan. 2024;2024(1): 4418466. https://doi.org/10.1155/2024/4418466.

[2] Kefeni KK, Msagati TAM, Nkambule TT, Mamba BB. Spinel ferrite nanoparticles and nanocomposites for biomedical applications and their toxicity. Mater Sci Eng C 2020;107(October 2019):110314. https://doi.org/10.1016/j.msec.2019.110314.

[3] Barabadi H, Noqani H, Jounaki K, Kashani AS, Ashouri F. Antidiabetic nanotherapeutics of bioengineered silver and gold nanomaterials : a state - of - the - art review. Nanomed J 2025;12(4):546–92. https://doi.org/10.22038/nmj.2025.81522.2027.

[4] Rotello VM. Nanoparticles: building blocks for nanotechnology. Springer Science & Business Media; 2004.

[5] Thakkar KN, Mhatre SS, Parikh RY. Biological synthesis of metallic nanoparticles. Nanomed Nanotechnol Biol Med 2010;6(2):257–62.

[6] Das M, Chatterjee S. Green synthesis of metal/metal oxide nanoparticles toward biomedical applications: boon or bane. In: Green synthesis, characterization and applications of nanoparticles. Elsevier; 2019. p. 265–301.

[7] Slimani C, Rais C. Advances in green chemistry: plant and microbial processes for sustainable nanoparticle synthesis, and their antimicrobial and anticancer applications. 2024. https://doi.org/10.22034/crl.2024.457614.1337.

[8] Blums E, Maiorov MM, Kronkalns G. Thermomagnetic properties of ferrofluids containing chemically coprecipitated Mn-Zn ferrite particles. IEEE Trans Magn 1993;29(6): 3267–9. https://doi.org/10.1109/20.281158.

[9] Soufi A, Hajjaoui H, Elmoubarki R, Abdennouri M, Qourzal S, Barka N. Spinel ferrites nanoparticles: synthesis methods and application in heterogeneous Fenton oxidation of organic pollutants – a review. Appl Surf Sci Adv 2021;6:100145. https://doi.org/10.1016/j.apsadv.2021.100145.

[10] Vedrtnam A, Kalauni K, Dubey S, Kumar A. A comprehensive study on structure, properties, synthesis and characterization of ferrites. AIMS Mater Sci 2020;7(6): 800–35. https://doi.org/10.3934/matersci.2020.6.800.

[11] Jabbar R, Sabeeh SH, Hameed AM. The effect of Mn+2 doping ratio on the sensing properties of CoFe2O4 nanoparticles for CO2 and NH3 gases. UPB Sci Bull Ser B Chem Mater Sci 2020;82(1):47–58.

[12] Jabbar Rihab, Shahatha Sara H, Taieh Nabil Kadhim, Magid Bushra, Showard Ansam F. Preparation and study of the effect of pH value on structural, morphological, electrical and magnetic properties of CoFe2O4 nanoparticles prepared by sol-gel precipitation method. Ceram Int 2024;50(17):31114–23. https://doi.org/10.1016/j.ceramint.2024.05.417.

[13] Mathew DS, Juang RS. An overview of the structure and magnetism of spinel ferrite nanoparticles and their synthesis in microemulsions. Chem Eng J 2007;129(1–3):51–65. https://doi.org/10.1016/j.cej.2006.11.001.

[14] Pullar RC. Hexagonal ferrites: a review of the synthesis, properties and applications of hexaferrite ceramics. Prog Mater Sci 2012;57(7):1191–334. https://doi.org/10.1016/j.pmatsci.2012.04.001.

[15] Geller S, Gilleo MA. The crystal structure and ferrimagnetism of yttrium-iron garnet, Y3Fe2(FeO4)3. J Phys Chem Solid 1957;3(1–2):30–6. https://doi.org/10.1016/0022-3697(57)90044-6.

[16] Gilleo MA, Geller S. Magnetic and crystallographic properties of substituted yttrium-iron garnet, 3Y2O3•xM2O3•(5-x)Fe2O3. Phys Rev 1958;110(1):73–8. https://doi.org/10.1103/PhysRev.110.73.

[17] Tomina Elena, Novikova Lyudmila, Kotova Alexandra, Meshcheryakova Anna, Krupskaya Victoria, Morozov Ivan, et al. ZnFe2O4/Zeolite nanocomposites for sorption extraction of Cu2+ from aqueous medium. AppliedChem 2023;3(4):452–76. https://doi.org/10.3390/appliedchem3040029.

[18] Din MI, Jabbar S, Najeeb J, Khalid R, Ghaffar T, Arshad M, et al. Green synthesis of zinc ferrite nanoparticles for photocatalysis of methylene blue. Int J Phytoremediation 2020;22(13):1440–7. https://doi.org/10.1080/15226514.2020.1781783.

[19] Abdulhamid ZM, Dabbawala Aasif A, Delclos Thomas, Straubinger Rainer, Rueping Magnus, Polychronopoulou Kyriaki, et al. Synthesis, characterization, and preliminary insights of ZnFe2O4 nanoparticles into potential applications, with a focus on gas sensing. Sci Rep 2023;13(1): 1–16. https://doi.org/10.1038/s41598-023-46960-w.

[20] Sharma RK, Ghose R. Synthesis and characterization of nanocrystalline zinc ferrite spinel powders by homogeneous precipitation method. Ceram Int 2015;41(10): 14684–91.

[21] Kombaiah K, Vijaya JJ, Kennedy LJ, Bououdina M. Studies on the microwave assisted and conventional combustion synthesis of Hibiscus rosa-sinensis plant extract based ZnFe2O4 nanoparticles and their optical and magnetic properties. Ceram Int 2016;42(2):2741–9. https://doi.org/10.1016/j.ceramint.2015.11.003.

[22] Hasan S, Azhdar B. Synthesis of nickel-zinc ferrite nanoparticles by the sol-gel auto-combustion method: study of crystal structural, cation distribution, and magnetic properties. Adv Condens Matter Phys 2022;2022. https://doi.org/10.1155/2022/4603855.

[23] Shahnavaz Z, Woi PM, Alias Y. Electrochemical sensing of glucose by reduced graphene oxide-zinc ferrospinels. Appl Surf Sci 2016;379:156–62.

[24] Matinise N, Kaviyarasu K, Mongwaketsi N, Khamlich S, Kotsedi L, Mayedwa N, et al. Green synthesis of novel zinc iron oxide (ZnFe 2 O 4) nanocomposite via Moringa Oleifera natural extract for electrochemical applications. Appl Surf Sci 2018;446:66–73. https://doi.org/10.1016/j.apsusc.2018.02.187.

[25] Qu Lina, Hou Xianhua, Mao Junwei, Ru Qiang, Hu Shejun, Liu Xiang, et al. 3-Dimensional cuboid structured ZnFe 2 O 4@ C nano-whiskers as anode materials for lithium-ion batteries based on the in situ graft polymerization method. RSC Adv 2016;6(99):96743–51.

[26] Mao J, Hou X, Chen H, Ru Q, Hu S, Lam K. Facile spray drying synthesis of porous structured ZnFe2O4 as high-performance anode material for lithium-ion batteries. J Mater Sci Mater Electron 2017;28(4): 3709–15.

[27] Kumar A, Gaurav, Malik AK, Tewary DK, Singh B. A review on development of solid phase microextraction fibers by sol-gel methods and their applications. Anal Chim Acta 2008;610(1):1–14. https://doi.org/10.1016/j.aca.2008.01.028.

[28] Livage J, Sanchez C, Henry M, Doeuff S. The chemistry of the sol-gel process. Solid State Ionics 1989;32–33(PART 2): 633–8. https://doi.org/10.1016/0167-2738(89)90338-X.

[29] Livage J. Sol-gel processes. Curr Opin Solid State Mater Sci 1997;2(2):132–8. https://doi.org/10.1016/s1359-0286(97)80057-5.

[30] Zhao Y. Co-precipitated Ni/Mn shell coated nano Cu-rich core structure: a phase-field study. J Mater Res Technol 2022;21:546–60. https://doi.org/10.1016/j.jmrt.2022.09.032.

[31] Nasrin S, Chowdhury FUZ, Hoque SM. Study of hyperthermia temperature of manganese-substituted cobalt nano ferrites prepared by chemical co-precipitation method for biomedical application. J Magn Magn Mater November 2018;479:126–34. https://doi.org/10.1016/j.jmmm.2019.02.010. 2019.

[32] Salih SJ, Mahmood WM. Review on magnetic spinel ferrite (MFe2O4) nanoparticles: from synthesis to application. Heliyon 2023;9(6):e16601. https://doi.org/10.1016/j.heliyon.2023.e16601.

[33] Zhang Hao, Hu Jianghan, Li Mingwei, Li Zhenhua, Yuan Ye, Yang Xueli, et al. Highly efficient toluene gas

sensor based on spinel structured hollow urchin-like core-shell ZnFe2O4 spheres. Sensors Actuators B Chem 2021; 349:130734. https://doi.org/10.1016/j.snb.2021.130734.
[34] Rouhani Z, Karimi-Sabet J, Mehdipourghazi M, Hadi A, Dastbaz A. Response surface optimization of hydrothermal synthesis of Bismuth ferrite nanoparticles under supercritical water conditions: application for photocatalytic degradation of Tetracycline. Environ Nanotechnol Monit Manag 2019;11:100198. https://doi.org/10.1016/j.enmm.2018.100198.
[35] Slimani Y, Almessiere MA, Guner S, Aktas B, Shirsath SE, Silibin Maxim V, et al. Impact of Sm3+ and Er3+ cations on the structural, optical, and magnetic traits of spinel cobalt ferrite nanoparticles: Comparison investigation. ACS Omega 2022;7(7):6292–301. https://doi.org/10.1021/acsomega.1c06898.
[36] Mohammed AJ, Hamdan SA. The influence of the various PH value on structural and magnetic properties of cobalt ferrite nanostracture. Mustansiriyah J Pure Appl Sci 2024;2: 15–30.
[37] Meydan E, Demirci S, Aktas N, Sahiner N, Ozturk OF. Catalytic performance of boron-containing magnetic metal nanoparticles in methylene blue degradation reaction and mixture with other pollutants. Inorg Chem Commun 2021; 126:108474. https://doi.org/10.1016/j.inoche.2021.108474.
[38] Sharifianjazi F, Moradi M, Parvin N, Nemati A, Rad AJ, Sheysi N, et al. Magnetic CoFe2O4 nanoparticles doped with metal ions: a review. Ceram Int 2020;46(11):18391–412. https://doi.org/10.1016/j.ceramint.2020.04.202.
[39] Liu S, Yu B, Wang S, Shen Y, Cong H. Preparation, surface functionalization and application of Fe3O4 magnetic nanoparticles. Adv Colloid Interface Sci 2020;281:102165. https://doi.org/10.1016/j.cis.2020.102165.
[40] Almessiere MA, Slimani Y, Guner S, Sertkol M, Demir Korkmaz A, Shirsath Sagar E, et al. Sonochemical synthesis and physical properties of Co0.3Ni0.5Mn0.2EuxFe2−xO4 nano-spinel ferrites. Ultrason Sonochem 2019;58:104654. https://doi.org/10.1016/j.ultsonch.2019.104654.
[41] Slimani Y, Almessiere MA, Demir Korkmaz A, Guner S, Güngüneş H, Sertkol M, et al. Ni0.4Cu0.2Zn0.4TbxFe2-xO4 nanospinel ferrites: ultrasonic synthesis and physical properties. Ultrason Sonochem 2019;59:104757. https://doi.org/10.1016/j.ultsonch.2019.104757.
[42] Ilosvai AM, Dojcsak D, Varadi C, Nagy M, Kristaly F, Fiser B, et al. Sonochemical combined synthesis of nickel ferrite and cobalt ferrite magnetic nanoparticles and their application in glycan analysis. 2022. https://doi.org/10.3390/ijms23095081.
[43] Strukil V. Mechanochemical synthesis of thioureas, ureas and guanidines. Beilstein J Org Chem 2017;13:1828–49. https://doi.org/10.3762/bjoc.13.178.
[44] Wei Leong Kean, Rahim Shayfull Zamree Abd, Abdullah Mohd Mustafa Al Bakri, Yin Allice Tan Mun, Ghazali Mohd Fathullah, Omar Mohd Firdaus, et al. Producing metal powder from machining chips using ball milling process: a review. Materials 2023;16(13). https://doi.org/10.3390/ma16134635.
[45] Blazquez JS, Ipus JJ, Moreno-Ramírez LM, Alvarez-Gomez JM, Sanchez-Jimenez D, Lozano-Perez S, et al. Ball milling as a way to produce magnetic and magnetocaloric materials: a review. J Mater Sci 2017;52(20):11834–50. https://doi.org/10.1007/s10853-017-1089-3.
[46] de Lima Barizao AC, de Oliveira JP, Gonçalves RF, Cassini ST. Nanomagnetic approach applied to microalgae biomass harvesting: advances, gaps, and perspectives. Environ Sci Pollut Res 2021;28(33):44795–811. https://doi.org/10.1007/s11356-021-15260-z.
[47] Piras CC, Fernandez-Prieto S, De Borggraeve WM. Ball milling: a green technology for the preparation and functionalisation of nanocellulose derivatives. Nanoscale Adv 2019;1(3):937–47. https://doi.org/10.1039/c8na00238j.
[48] Kumari R, Banik SK, Roy S, Ahmaruzzaman M. Recent developments in eco-friendly synthesis of ZnFe2O4 and its composites for multidimensional applications: innovations and future directions. Inorg Chem Commun 2025;182(P2): 115560. https://doi.org/10.1016/j.inoche.2025.115560.
[49] Jabbar Rihab. Green synthesis of cobalt ferrite nanoparticles: from fundamentals to advanced applications. Next Mater 2025;9:101327. https://doi.org/10.1016/j.nxmate.2025.101327 [Online]. Available:.
[50] Jamal Salih S. Green synthesis and characterization of polyphenol-coated magnesium-substituted manganese ferrite nanoparticles: antibacterial and antioxidant properties. Heliyon May 2024;10(10):e31428. https://doi.org/10.1016/j.heliyon.2024.e31428.
[51] Sahoo P, Choudhary P, Laha SS, Dixit A, Mefford OT. Recent advances in zinc ferrite (ZnFe2O4) based nanostructures for magnetic hyperthermia applications. Chem Commun 2023;59(81):12065–90. https://doi.org/10.1039/d3cc01637d.
[52] Dahoumane SA, Jeffryes C, Mechouet M, Agathos SN. Biosynthesis of inorganic nanoparticles: a fresh look at the control of shape, size and composition. Bioengineering 2017;4(1):1–16. https://doi.org/10.3390/bioengineering4010014.
[53] Villagran Zuamí, Anaya-Esparza Luis Miguel, Arnulfo Velazquez-Carriles Carlos, Silva-Jara Jorge Manuel, Martín Ruvalcaba-Gomez Jose, Aurora-Vigo Edward F, et al. Plant-based extracts as reducing, capping, and stabilizing agents for the green synthesis of inorganic nanoparticles. 2024. https://doi.org/10.3390/resources13060070.
[54] Muthukumar H, Palanirajan SK, Shanmugam MK, Gummadi SN. Plant extract mediated synthesis enhanced the functional properties of silver ferrite nanoparticles over chemical mediated synthesis. Biotechnol Rep (Amsterdam, Netherlands) Jun. 2020;26:e00469. https://doi.org/10.1016/j.btre.2020.e00469.
[55] Matinise N. Recent advances review in plant extracts-driven green synthesis of binary-metal oxide nanomaterials for sustainable nanotechnology. Scientifica (Cairo) 2025;2025:2888408. https://doi.org/10.1155/sci5/2888408.
[56] Bouttier-Figueroa DC, Cortez-Valadez JM, Flores-Acosta M, Robles-Zepeda RE. Synthesis of metallic nanoparticles using plant's natural extracts: synthesis mechanisms and applications. Biotecnia 2023;25(3):125–39. https://doi.org/10.18633/biotecnia.v25i3.1916.
[57] Singh P, Kim Y-J, Zhang D, Yang D-C. Biological synthesis of nanoparticles from plants and microorganisms. Trends Biotechnol Jul. 2016;34(7):588–99. https://doi.org/10.1016/j.tibtech.2016.02.006.
[58] Iravani S. Green synthesis of metal nanoparticles using plants. Green Chem 2011;13(10):2638–50. https://doi.org/10.1039/C1GC15386B.
[59] Singh H, Desimone Martin F, Pandya Shivani, Jasani Srushti, George Noble, Adnan Mohd, et al. Revisiting the green synthesis of nanoparticles: uncovering influences of plant extracts as reducing agents for enhanced synthesis efficiency and its biomedical applications. Int J Nanomed 2023;18(August):4727–50. https://doi.org/10.2147/IJN.S419369.
[60] Lee Jaewook, Kim Hyeon Yong, Zhou Hongjian, Hwang Sungu, Koh Kwangnak, Han Dong-Wook, Lee Jaebeom. Green synthesis of phytochemical-stabilized Au nanoparticles under ambient conditions and their biocompatibility and antioxidative activity. J Mater Chem 2011;21(35):13316–26. https://doi.org/10.1039/c1jm11592h.
[61] Gebre SH. Bio-inspired synthesis of metal and metal oxide nanoparticles: the key role of phytochemicals. Springer US 2023;34(2). https://doi.org/10.1007/s10876-022-02276-9.
[62] Sheydaei M, Shahbazi-Ganjgah S, Alinia-Ahandani E, Sheidaie M, Edraki M. An overview of the use of plants, polymers and nanoparticles as antibacterial materials.

Chem Rev Lett 2022;5(3):207–16. https://doi.org/10.22034/CRL.2022.343015.1168.
[63] Egamberdieva D, Jabborova D, Babich S, Xalmirzaeva S, Salakhiddinov K, Madazimov M. Antimicrobial activities of herbal plants from Uzbekistan against human pathogenic microbes. Environ Sustain 2021;4:87–94.
[64] Rostami-Vartooni A, Nasrollahzadeh M, Alizadeh M. Green synthesis of seashell supported silver nanoparticles using Bunium persicum seeds extract: application of the particles for catalytic reduction of organic dyes. J Colloid Interface Sci 2016;470:268–75. https://doi.org/10.1016/j.jcis.2016.02.060.
[65] Tatarchuk T, Maria L, Volodymyr K, Bououdina M. Green synthesis of cobalt ferrite nanoparticles using Cydonia oblonga extract: structural and mossbauer studies. Mol Cryst Liq Cryst Sep. 2018;672(1):54–66. https://doi.org/10.1080/15421406.2018.1542107.
[66] Abdel-Aziz HM, Farag RS, Abdel-Gawad SA. Carbamazepine removal from aqueous solution by green synthesis zero-valent Iron/Cu nanoparticles with Ficus Benjamina leaves' extract. Int J Environ Res 2019;13(5):843–52. https://doi.org/10.1007/s41742-019-00220-w.
[67] Sivakami M, Renuka Devi K, Renuka R, Thilagavathi T. Green synthesis of magnetic nanoparticles via Cinnamomum verum bark extract for biological application. J Environ Chem Eng 2020;8(5):104420. https://doi.org/10.1016/j.jece.2020.104420.
[68] Gingasu Dana, Culita Daniela C, Moreno Jose Maria Calderon, Marinescu Gabriela, Bartha Cristina, Oprea Ovidiu, et al. Synthesis of CoFe 2 O 4 through wet ferritization method using an aqueous extract of eucalyptus leaves. 2023. p. 1–15.
[69] Soltys L, Olkhovyy O, Tatarchuk T, Naushad M. Green synthesis of metal and metal oxide nanoparticles: principles of green chemistry and raw materials. 2021. https://doi.org/10.3390/magnetochemistry7110145.
[70] Tuama MJ, Alias MF. Synthesis of ZnO: ZrO2 nanocomposites using green method for medical applications. Karbala Int J Mod Sci 2024;10(3):418–30. https://doi.org/10.33640/2405-609X.3366.
[71] Laokul P, Amornkitbamrung V, Seraphin S, Maensiri S. Characterization and magnetic properties of nanocrystalline CuFe 2O4, NiFe2O4, ZnFe2O 4 powders prepared by the Aloe vera extract solution. Curr Appl Phys 2011;11(1):101–8. https://doi.org/10.1016/j.cap.2010.06.027.
[72] Sarala E, Madhukara Naik M, Vinuth M, Rami Reddy YV, Sujatha HR. Green synthesis of Lawsonia inermis-mediated zinc ferrite nanoparticles for magnetic studies and anticancer activity against breast cancer (MCF-7) cell lines. J Mater Sci Mater Electron 2020;31(11):8589–96. https://doi.org/10.1007/s10854-020-03394-8.
[73] Kombaiah K, Vijaya JJ, Kennedy LJ, Bououdina M, Al-Lohedan HA, Ramalingam RJ. Studies on opuntia dilenii haw mediated multifunctional ZnFe2O4 nanoparticles: optical, magnetic and catalytic applications. Mater Chem Phys 2017;194:153–64. https://doi.org/10.1016/j.matchemphys.2017.03.020.
[74] Phumying S, Labuayai S, Swatsitang E, Amornkitbamrung V, Maensiri S. Nanocrystalline spinel ferrite (MFe2O4, M = Ni, Co, Mn, Mg, Zn) powders prepared by a simple aloe vera plant-extracted solution hydrothermal route. Mater Res Bull 2013;48(6):2060–5. https://doi.org/10.1016/j.materresbull.2013.02.042.
[75] Gayathri Manju B, Raji P. Green synthesis of nickel–copper mixed ferrite nanoparticles: structural, optical, magnetic, electrochemical and antibacterial studies. J Electron Mater 2019;48(12):7710–20. https://doi.org/10.1007/s11664-019-07603-x.
[76] Madhukara Naik M, Bhojya Naik HS, Nagaraju G, Vinuth M, Raja Naika H, Vinu K. Green synthesis of zinc ferrite nanoparticles in Limonia acidissima juice: characterization and their application as photocatalytic and antibacterial activities. Microchem J 2019;146(December 2018):1227–35. https://doi.org/10.1016/j.microc.2019.02.059.
[77] Korotkova AM, Polivanova OB, Gavrish IA, Baranova EN, Lebedev SV. Green synthesis of zinc based nanoparticles zinc ferrite by Petroselinum crispum. IOP Conf Ser Earth Environ Sci 2019;341(1). https://doi.org/10.1088/1755-1315/341/1/012175.
[78] Lakshmi Ranganatha V, Pramila S, Nagaraju G, Udayabhanu, Surendra BS, Mallikarjunaswamy C. Cost-effective and green approach for the synthesis of zinc ferrite nanoparticles using Aegle Marmelos extract as a fuel: catalytic, electrochemical, and microbial applications. J Mater Sci Mater Electron 2020;31(20):17386–403. https://doi.org/10.1007/s10854-020-04295-6.
[79] Sriramulu M, Shukla D, Sumathi S. Aegle marmelos leaves extract mediated synthesis of zinc ferrite: antibacterial activity and drug delivery. Mater Res Express 2018;5(11):1–9. https://doi.org/10.1088/2053-1591/aadd88.
[80] Selvam NCS, Kumar RT, Kennedy LJ, Vijaya JJ. Comparative study of microwave and conventional methods for the preparation and optical properties of novel MgO-micro and nano-structures. J Alloys Compd 2011;509(41):9809–15. https://doi.org/10.1016/j.jallcom.2011.08.032.
[81] Tatarchuk Tetiana, Shyichuk Alexander, Sojka Zbigniew, Grybos Joanna, Naushad Mu, Kotsyubynsky Volodymyr, et al. Green synthesis, structure, cations distribution and bonding characteristics of superparamagnetic cobalt-zinc ferrites nanoparticles for Pb(II) adsorption and magnetic hyperthermia applications. J Mol Liq 2021;328. https://doi.org/10.1016/j.molliq.2021.115375.
[82] Omelyanchik Alexander, Levada Kateryna, Pshenichnikov Stanislav, Abdolrahim Maryam, Baricic Miran, Kapitunova Anastasiya, et al. Green synthesis of co-zn spinel ferrite nanoparticles: magnetic and intrinsic antimicrobial properties. Materials 2020;13(21):1–13. https://doi.org/10.3390/ma13215014.
[83] Patil SB, Bhojya Naik HS, Nagaraju G, Viswanath R, Rashmi SK, Vijay kumar M. Sugarcane juice mediated eco-friendly synthesis of visible light active zinc ferrite nanoparticles: application to degradation of mixed dyes and antibacterial activities. Mater Chem Phys 2018;212:351–62. https://doi.org/10.1016/j.matchemphys.2018.03.038.
[84] Harisha G, Thejas R, Padmini BV, Devaraja CR, Murugendrappa MV, Rajashekara KM. Structural, morphological, magnetic, and dielectric properties of copper-substituted CuXZn(1-X)Fe2O4 nanoparticles: green synthesis. J Met Mater Miner 2024;34(3):1–7. https://doi.org/10.55713/JMMM.V34I3.1955.
[85] Adawiah A, Zulys A, Fitria I, Khalil M, Aziz I, Khalid M. Perylene-based metal-organic frameworks-decorated Zinc Ferrite for enhanced photodegradation of malachite green in aqueous system. South Afr J Chem Eng 2025;53(March):319–30. https://doi.org/10.1016/j.sajce.2025.05.005.
[86] Saridewi Nanda, Utami Dienda Juita, Zulys Agustino, Nurbayti Siti, Nurhasni, Adawiah, et al. Utilization of Lidah mertua (Sansevieria trifasciata) extract for green synthesis of ZnFe2O4 nanoparticle as visible-light responsive photocatalyst for dye degradation. Case Stud Chem Environ Eng 2024;9(April):100745. https://doi.org/10.1016/j.cscee.2024.100745.
[87] Prabhakaran T, V Mangalaraja R, Denardin JC, Varaprasad K. The effect of capping agents on the structural and magnetic properties of cobalt ferrite nanoparticles. J Mater Sci Mater Electron 2018;29(14):11774–82. https://doi.org/10.1007/s10854-018-9276-9.
[88] Taghavi Fardood S, Ramazani A, Golfar Z, Joo SW. Green synthesis of ni-cu-zn ferrite nanoparticles using tragacanth gum and their use as an efficient catalyst for the synthesis of polyhydroquinoline derivatives. Appl Organomet Chem 2017;31(12):1–7. https://doi.org/10.1002/aoc.3823.
[89] Najm ZA, Atiya MA, Hassan AK. Adsorption and photocatalytic of biosynthesis zinc ferrite nanoparticles for removing acid Black 210 dye from aqueous medium.

Baghdad Sci J 2025;22(3):756–70. https://doi.org/10.21123/bsj.2024.9359.
[90] Jabbar R, Alluaibi, Ismail Mohammed Hayder, Shahatha SH. Green pepper extract-based biosynthesis of NiFe2O4 and ZnFe2O4: a mechanistic structure, physicochemical–property correlation for potential multifunctional applications. Mater Sci Eng B 2026;328:119365. https://doi.org/10.1016/j.mseb.2026.119365 [Online]. Available:.
[91] Lithi IJ, Ahmed Nakib KI, Chowdhury AMS, Sahadat Hossain M. A review on the green synthesis of metal (Ag, Cu, and Au) and metal oxide (ZnO, MgO, Co3O4, and TiO2) nanoparticles using plant extracts for developing antimicrobial properties. Nanoscale Adv 2025;7(9):2446–73. https://doi.org/10.1039/d5na00037h.
[92] Younas Umer, Fatima Zumer, Saleem Aimon, Zaki I Zaki, Ali Faisal, Pervaiz Muhammad, et al. Kinetic studies of catalytic and antioxidant activities of biosynthesized franklinite (ZnFe2O4) nanoparticles using Coriandrum sativum leaf extract 2023;237(10):1559–74. https://doi.org/10.1515/zpch-2023-0254.
[93] Nguyen NTT, Nguyen TTT, Nguyen DTC, Van Tran T. Green synthesis of ZnFe2O4 nanoparticles using plant extracts and their applications: a review. Sci Total Environ May 2023;872:162212. https://doi.org/10.1016/j.scitotenv.2023.162212.
[94] Takcõ DK, Ozdenefe MS, Huner T, Takcõ HAM. Plant-mediated green route to the synthesis of zinc oxide nanoparticles: in vitro antibacterial potential. J Australas Ceram Soc 2025;61(1):31–9. https://doi.org/10.1007/s41779-024-01064-0.
[95] Adawiah A, Oktavia W, Saridewi N, Azhar FM, Fitria RN, Gunawan MS, et al. Synthesis metal-organic framework (MOFs) Cr-PTC-HIna modulated isonicotinic acid for methylene blue Photocatalytic degradation. Bull Chem React Eng Catal 2022 BCREC 2022;17(2). https://doi.org/10.9767/bcrec.17.2.13930.383-393. Jun. 2022, [Online]. Available: https://journal.bcrec.id/index.php/bcrec/article/view/13930.
[96] Manjura Hoque S, Sazzad Hossain Md, Choudhury Shamima, Akhter S, Hyder F. Synthesis and characterization of ZnFe2 O4 nanoparticles and its biomedical applications S. Physiol Behav 2017;176(3):139–48. https://doi.org/10.1002/hep.30150.Ductular.
[97] Nguyen NTT, Nguyen TTT, Nguyen DTC, Van Tran T. Green synthesis of ZnFe(2)O(4) nanoparticles using plant extracts and their applications: a review. Sci Total Environ May 2023;872:162212. https://doi.org/10.1016/j.scitotenv.2023.162212.
[98] Frtús Adam, Smolkova Barbora, Uzhytchak Mariia, Lunova Mariia, Jirsa Milan, Kubinova Sarka, et al. Analyzing the mechanisms of iron oxide nanoparticles interactions with cells: a road from failure to success in clinical applications. J Contr Release 2020;328:59–77. https://doi.org/10.1016/j.jconrel.2020.08.036.
[99] Rodrigues GR, Lopez-Abarrategui C, de la Serna Gomez I, Dias SC, Otero-Gonzalez AJ, Franco OL. Antimicrobial magnetic nanoparticles based-therapies for controlling infectious diseases. Int J Pharm 2019;555:356–67. https://doi.org/10.1016/j.ijpharm.2018.11.043.
[100] Muhanad Alhujaily, Jabir Majid S, Nayef Uday M, Rashid Taha M, Sulaiman Ghassan M, Khalil Khalil AA, et al. Au/ZnO nanocomposites prepared by laser ablation for enhancement of antibacterial activity and cytotoxic properties against cancer cells. Metals 2023;13(4). https://doi.org/10.3390/met13040735.
[101] Mohammed Mahdi A, Abdulkadhim Waleed K, Jawad Kareem H, Albukhaty Salim, Jabir Majid S, Ghotekar Suresh, et al. Magnetically enhanced ZnFe2O4 nanocomposite: a promising antibacterial, and antioxidant strategies. J Sol Gel Sci Technol 2025;115(3):1557–66.
[102] Jacobson Kurt H, Gunsolus Ian L, Kuech Thomas R, Troiano Julianne M, Melby Eric S, Lohse Samuel E, et al. Lipopolysaccharide density and structure govern the extent and distance of nanoparticle interaction with actual and model bacterial outer membranes. Environ Sci Technol Sep. 2015;49(17):10642–50. https://doi.org/10.1021/acs.est.5b01841.
[103] Nikaido H. Outer membrane barrier as a mechanism of antimicrobial resistance. Antimicrob Agents Chemother 1989;33(11):1831–6.
[104] Alfei S, Schito GC, Schito AM, Zuccari G. Reactive oxygen species (ROS)-mediated antibacterial oxidative therapies: available methods to generate ROS and a novel option proposal. Int J Mol Sci 2024;25(13). https://doi.org/10.3390/ijms25137182.
[105] Ashley Jonathan D, Quinlan Charissa J, Schroeder Valerie A, Suckow Mark A, Pizzuti Vincenzo J, Kiziltepe Tanyel, Bilgicer Basar. Dual carfilzomib and Doxorubicin–loaded liposomal nanoparticles for synergistic efficacy in multiple myeloma. Mol Cancer Therapeut Jul. 2016;15(7):1452–9. https://doi.org/10.1158/1535-7163.MCT-15-0867.
[106] Wang Guangshuo, Ma Yingying, Zhang Lina, Mu Jingbo, Zhang Zhixiao, Zhang Xiaoliang, et al. Facile synthesis of manganese ferrite/graphene oxide nanocomposites for controlled targeted drug delivery. J Magn Magn Mater 2016;401:647–50. https://doi.org/10.1016/j.jmmm.2015.10.096.
[107] Imraish A, Al-Hunaiti A, Abu-Thiab T, Ibrahim AA-Q, Hwaitat E, Omar A. Phyto-facilitated bimetallic ZnFe(2)O(4) nanoparticles via Boswellia carteri: synthesis, characterization, and anti-cancer activity. Anti Cancer Agents Med Chem 2021;21(13):1767–72. https://doi.org/10.2174/1871520621666201218114040.
[108] Elgendy K, Elmehasseb I, Kandil S. Efficient removal of common organic pollutants from water by Zn-doped TiO2 nanoparticles with different applications. Karbala Int J Mod Sci 2022;8(2):223–36. https://doi.org/10.33640/2405-609X.3226.
[109] El Messaoudi Noureddine, Cigeroglu Zeynep, Şenol Zeynep Mine, Bouich Amal, Kazan-Kaya Emine Sena, Noureen Laila, et al. Green synthesis of nanoparticles for remediation organic pollutants in wastewater by adsorption. In: Kumar A, Bilal M, L. F. R. B. T.-A, Ferreira CP, editors. Recent advancements in wastewater management: nano-Based remediation. 10. Elsevier; 2024. p. 305–45. https://doi.org/10.1016/bs.apmp.2023.06.016. Environmental management and protection.
[110] Yi J-Z, Zhang L-M. Removal of methylene blue dye from aqueous solution by adsorption onto sodium humate/polyacrylamide/clay hybrid hydrogels. Bioresour Technol 2008;99(7):2182–6.
[111] Ahmad M, Ahmed E, Ahmed W, Elhissi A, Hong ZL, Khalid NR. Enhancing visible light responsive photocatalytic activity by decorating Mn-doped ZnO nanoparticles on graphene. Ceram Int 2014;40(7):10085–97.
[112] Kumar V, Singh Y, Kaushal S, Kumar R. Bioinspired synthesis of copper oxide nanoparticles using aqueous extracts of Cladophora glomerata (L.) Kuetz and their potential biomedical applications. Bioproc Biosyst Eng 2025;48(4):633–46. https://doi.org/10.1007/s00449-025-03133-5.
[113] Sadeghifar AR, Farsinejad A, Satarzadeh N, Shahabi A, Sadeghi Dousari A. Biosynthesized metal nanoparticles as a high-potential tool in bone regenerative medicine: a review. Biol Trace Elem Res 2025. https://doi.org/10.1007/s12011-025-04800-0.